INVITED PAPER

PACS numbers: 32.80.Pj, 32.10.Dk, 31.15.Ar, 31.25.Jf; 42.62.Eh
DOI: 10.1070/QE2006v036n01ABEH013098

Polarisation and dispersion properties of light shifts in ultrastable optical frequency standards

V.D. Ovsiannikov, V.G. Pal'chikov, H. Katori, M. Takamoto

***Abstract*. The theoretical aspects of the Stark spectroscopy of cold alkaline-earth atoms in a three-dimensional optical lattice related to the development of ultrastable optical frequency standards of a new generation are considered. The main attention is devoted to the dispersion and polarisation properties of the light frequency shift in these atoms, which depend on the power, frequency, and polarisation of lasers forming the optical lattice. The 'light-shift-cancellation' regime is considered in detail, in which the second-order dynamic Stark shifts at the forbidden clock $^3P_0 - {}^1S_0$ and $^3P_1 - {}^1S_0$ transitions are mutually compensated. The wavelengths at which this regime takes place ('magic' wavelengths) are calculated for the He, Be, Mg, Ca, Sr, Yb, and Hg atoms. The fourth-order dynamic susceptibilities (hyperpolarisabilities) are calculated for Sr atoms and the contribution of higher-order multipole corrections to the dynamic polarisability of the $^3P_0$ and $^1S_0$ levels is estimated.**

Keywords: *optical lattice, forbidden transitions, cold atoms, light shift, optical frequency standards.*

1. Introduction

The basic metrological parameters characterising the primary time and frequency standards are the accuracy of frequency measuring, its reproducibility and stability. At present the frequency standards of a new generation – atomic fountains developed in the last decade in a number of leading laboratories worldwide {NIST (F1) [1], PTB (CSF1) [2], SYRTE (FO2, FOM) [3, 4], IEN (CsF1) [5], NPL (CsF1) [6]}, have the best accuracy. Compared to classical primary microwave cesium atom standards (see, for example, [7 – 9]), the accuracy of independent reproducibility of the time and frequency units in atomic fountains is at least an order of magnitude better, amounting to $\sim 10^{-16}$, while the long-term stability is $\sim 10^{-15}$ per day [10].

In the last few years a qualitatively new stage in the development of optical frequency standards began, which is based on the use of femtosecond lasers for the elaboration of optical clocks and synthesis and precision measurements of absolute frequencies in the optical range [11 – 14]. A femtosecond laser emits a set of equidistant frequency components separated by a 100 MHz – 1 GHz frequency comb, which fill the entire emission spectrum of the laser (up to hundreds of terahertz). The intermode intervals are equidistant within an error of no worse than $10^{-16} - 10^{-17}$, which is provided by the self-mode-locking process itself [15 – 17]. Therefore, to obtain a frequency comb in a broad spectral range, it is sufficient to lock any of the components of a comb generator to a frequency standard used as a reference. Applications of femtosecond lasers for absolute measurements of optical frequencies are considered in [17 – 21].

An alternative to atomic fountains for precision time and frequency measurements may be at present optical standards based on cold neutral atoms or singly ionised ions (see, for example, [22 – 27]). Without considering in detail the advantages and disadvantages inherent in standards of this type, we will point out here their most important specific properties determining a rapidly increasing interest in the development of optical frequency references based on various schemes of laser cooling and trapping of atoms.

First, one of the most important advantages of optical standards is a higher frequency of the so-called clock transitions used in them (hundreds and thousands of terahertz), which in turn makes it possible to achieve a higher (by a few orders of magnitude) relative frequency stability due to an increase in the cavity Q factor ($10^{12} - 10^{14}$ [28]). Thus, in optical frequency standards on Hg^+ ions and Ca atoms, in which the electric quadrupole transition

$$^2S_{1/2}(F = 0, M_F = 0) - {}^2D_{5/2}(F = 0, M_F = 0)\ (\lambda = 282\ \text{nm})$$

and the intercombination transition

$$^1S_0(M = 0) - {}^3P_1(M = 0)\ (\lambda = 657\ \text{nm}),$$

are used as frequency references, the relative frequency stability is estimated as 1×10^{-15} and 1.6×10^{-16} per second, respectively, while a similar estimate for the 698-nm $5s^2\,{}^1S_0(F = 9/2) - 5s5p\,{}^3P_0(F = 9/2)$ transition in fre-

V.D. Ovsiannikov Department of Physics, Voronezh State University, Universitetskaya pl. 1, 394006 Voronezh, Russia;
e-mail: ovd@phys.vsu.ru;
V.G. Pal'chikov All-Russia Research Institute for Physical-Technical and Radiotechnical Measurements, Institute of Metrology for Time and Space, 141570 Mendeleevo, Moscow region; e-mail: vitpal@mail.ru;
H. Katori, M. Takamoto Department of Applied Physics, School of Engineering, University of Tokyo, Bunkyo-ku, 113-8656 Tokyo, Japan; e-mail: katori@ato.t.u-tokyo.ac.jp

Received 29 August 2005
Kvantovaya Elektronika **36** (1) 3 – 19 (2006)
Translated by M.N. Sapozhnikov

quency standards based on the fermion isotope of a strontium atom (^{87}Sr) gives $\sim 1 \times 10^{-18}$ per second [25]. It follows from these estimates that the optical frequency standard has an advantage over the microwave fountain frequency standard because it has a significantly higher stability for a shorter measurement time.

Second, atomic systems with several valence outer-shell electrons used in optical standards as working media have rather complicated spectra containing narrow lines corresponding to strongly forbidden transitions in the optical range. For example, in the fermion isotopes of alkaline-earth atoms, along with the $^1S_0 - {}^3P_1$ intercombination transition, the above-mentioned $5s^2\,{}^1S_0(F = 9/2) - 5s5p\,{}^3P_0(F = 9/2)$ transition is used, which is caused by the hyperfine structure effects and singlet–triplet mixing of atomic $^3P_1$ and $^1P_1$ levels.

Katori and co-authors (University of Tokyo, Japan) [24, 25, 29–31] have recently realised experimentally the idea of localisation of cold Sr atoms in periodic spatial structures with dimensions less than the wavelength of light, which were produced in a standing laser radiation wave (optical lattices). This idea was first proposed by Letokhov [32] for reducing the Doppler width in the emission spectra of atoms. In this method, atoms trapped in a spatial region with dimensions much smaller than the wavelength of light emit a spectrum in which the Doppler broadening is strongly suppressed, i.e., their fluorescence lines are narrowed due to the Lamb–Dicke effect [33]. As follows from Fig. 1 [25], the $5s^2\,{}^1S_0(F = 9/2) - 5s5p\,{}^3P_0(F = 9/2)$ transitions at a wavelength of 698 nm occur between the energy levels of atoms in fixed vibrational states in the potential well of the optical lattice. The primary laser cooling of Sr atoms is performed at the 461-nm $^1S_0 - {}^1P_1$ resonance transition; as a result, a part of atoms undergo transitions to the $5s5p\,{}^3P_2$ and $5s5p\,{}^3P_1$ triplet levels via the intermediate $5s4d\,{}^1D_2$ level. The secondary, deeper laser cooling (down to a few hundreds of nanokelvin) is performed at the $5s^2\,{}^1S_0(F = 9/2) - 5s5p\,{}^3P_1(F = 9/2)$ intercombination transition [34]. The optical lattice shown in Fig. 1 is formed in a standing wave of linearly polarised laser radiation at $\lambda_0 \approx 800$ nm [25, 31].

It is clear from the general physical considerations that the potential of the optical lattice localising an atom can noticeably perturb both the internal and external degrees of freedom of the atom (dynamic Stark shift of atomic levels, modulation of its position and velocity, etc.). It is the internal degrees of freedom that are of most fundamental and practical interest in optical frequency standards of this type because the accuracy of measuring the clock transition frequency depends first of all on the degree of action of factors perturbing the atomic levels and shifting the transition frequency with respect to its nominal value in the ideal case.

The authors of papers [24, 25, 29–31] proposed the original method to reduce to a minimum the effect of the optical-lattice potential on the measured $^1S_0 - {}^3P_J$ ($J = 0, 1$) transition frequency in the Sr atom. It was shown theoretically [25] and experimentally [31] that, by selecting properly the parameters of laser radiation (polarisation and frequency) producing an optical lattice, a complete mutual compensation of quadratic Stark shifts of the ground and excited atomic levels can be achieved ('light-shift-cancellation' regime). This method considerably reduces the measurement error related to the influence of the lattice potential on the frequency of optical transitions in alkaline-earth atoms, which makes the use of this approach urgent for the development of highly stable frequency standards in the optical range.

The primary aim of this paper is to study theoretically the polarisation and dispersion properties of light frequency shifts at the forbidden $^1S_0 - {}^3P_J$ ($J = 0, 1$) transitions in alkaline-earth atoms used in modern optical frequency standards employing optical lattices. We calculated the dynamic polarisabilities and hyperpolarisabilities of atomic levels as functions of the parameters of the laser field of the optical lattice by using the general quasi-stationary pertur-

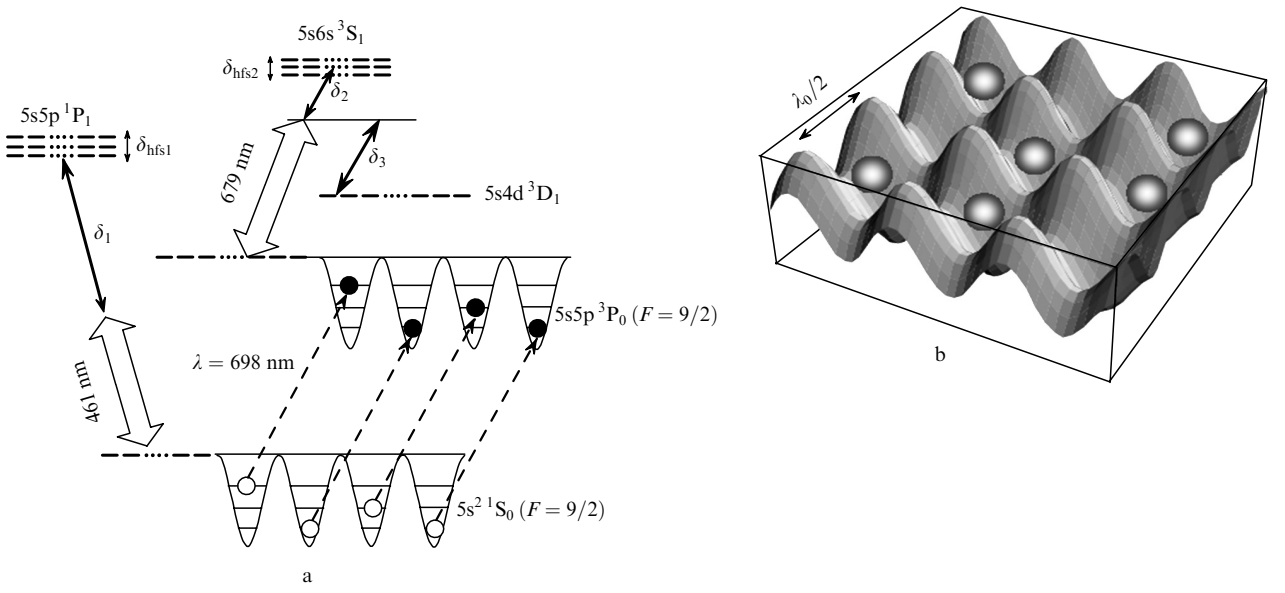

Figure 1. Scheme of optical transitions in the Sr atom (a) and a three-dimensional optical lattice in a linearly polarised laser field (b) [25]. δ_{1-3} are laser-frequency detunings from the transition centre; δ_{hfs1} and δ_{hfs2} are the hyperfine structure components of the states; $\lambda_0/2$ is the optical lattice period.

bation theory. We discussed in detail the results of calculations of the 'magic' wavelengths of laser radiation at which the light-shift-cancellation regime is realised, which minimises the effect of the localising potential on the frequency shift of the $^1S_0 - {}^3P_J$ ($J = 0, 1$) clock transitions in alkaline-earth atoms.

2. Radiative probabilities of forbidden transitions in alkaline-earth atoms

As pointed out in Introduction, the spectra of alkaline-earth atoms contain intercombination and forbidden transition lines with very small natural widths, which make them convenient for using as clock transitions in modern highly stable optical frequency standards on cold atoms. Figure 2 presents a simplified scheme of low-lying levels of an alkaline-earth atom showing possible radiative decay channels.

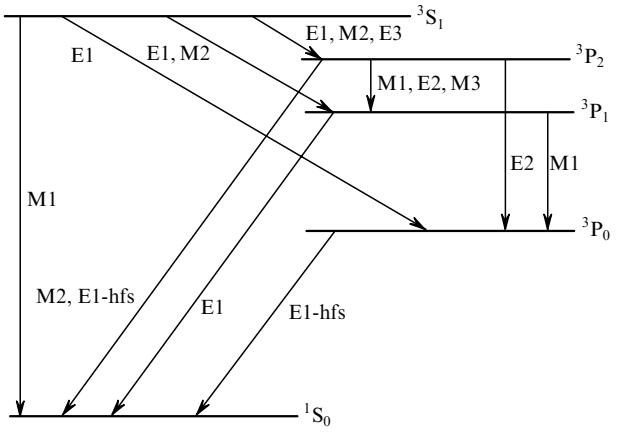

Figure 2. Diagram of optical multipole transitions in alkaline-earth atoms.

The natural width $\Delta\nu$ of the atomic transition from the excited state $|k\rangle$ to the ground state $|i\rangle$ is related to the spontaneous emission rate (transition probability per unit time, or the Einstein coefficient) A_{ki} by the expression

$$\Delta\nu = \frac{A_{ki}}{2\pi}. \tag{1}$$

It is convenient to express the coefficient A_{ki} in terms of the line strength S (Table 1). In Table 1, $g_k = 2J_k + 1$ is the statistic weight for the excited level $|k\rangle$. In the atomic system of units, the line strength is written as the square of the reduced matrix element of the operator of interaction with the radiation field [35, 36]:

$$S_{E1} = |\langle i\|\boldsymbol{D}\|k\rangle|^2, \quad S_{E2} = |\langle i\|Q_2\|k\rangle|^2,$$

$$S_{M1} = |\langle i\|\boldsymbol{L} + 2\boldsymbol{S}\|k\rangle|^2, \tag{2}$$

$$S_{M2} = |\langle i\|\{(\boldsymbol{L} + 2\boldsymbol{S}) \otimes \boldsymbol{D}\}_2\|k\rangle|^2,$$

where $\boldsymbol{D}$, Q_2, $\boldsymbol{L}$ and $\boldsymbol{S}$ are the electric dipole, electric quadrupole, orbital, and spin moments of an atom; and $\{\boldsymbol{a} \otimes \boldsymbol{b}\}_2$ are the second-rank irreducible tensor product of two vectors. The general theory and multiconfiguration approach to the calculation of the line strengths and probabilities of multipole transitions in atoms with two valence electrons are considered, for example, in [35–37].

Table 1. Relation between A_{ki} and the line strength S (in atomic units) for electric and magnetic dipole transitions followed by radiation at the wavelength λ (in Angström).

Transition type	$A_{ki}/\,s^{-1}$
E1	$[2.026 \times 10^{18}/(g_k\lambda^3)]S_{E1}$
E2	$[1.120 \times 10^{18}/(g_k\lambda^5)]S_{E2}$
M1	$[2.697 \times 10^{13}/(g_k\lambda^3)]S_{M1}$
M2	$[1.491 \times 10^{13}/(g_k\lambda^5)]S_{M2}$

The results of calculations of probabilities of one-photon transitions from the $^3P_2$ level show that the dominating decay channel for Mg and Ca atoms is the magnetic quadrupole (M2) transition to the ground state (Fig. 2 and Table 2). For the Sr atom, however, the most probable is the magnetic dipole (M1) $^3P_2 - {}^3P_1$ transition between the sublevels of the fine structure of the atomic multiplet (Fig. 2). If the probability of a given radiative transition is calculated in the nonrelativistic approximation, the Einstein coefficient A_{M1} (in atomic units) will be determined by a simple analytic expression [38]

$$A_{M1} = \frac{1}{6}\alpha^5\omega_{M1}^3, \tag{3}$$

where $\alpha = 1/137.0360$ is the fine structure constant and ω_{M1} is the M1 atomic transition frequency.

Table 2. Calculated and experimental probabilities of forbidden transitions for isotopes of alkaline-earth atoms with the zero nuclear spin.

Transition	Transition type	$A_{ki}^{calc}/\,s^{-1}$			$A_{ki}^{exp}/\,s^{-1}$		
		Mg	Ca	Sr	Mg	Ca	Sr
$^3P_1 - {}^1S_0$	E1	2.6×10^2 [37] 2.8×10^2 [40]	2.4×10^3 [37] 2.7×10^3 [40]	5.5×10^4 [37] 5.3×10^4 [40]	$1.9(3) \times 10^2$ [41] $2.1(4) \times 10^2$ [42] $2.5(1.2) \times 10^2$ [43]	$2.98(8) \times 10^3$ [44] $2.9(2) \times 10^3$ [45] $2.9(3) \times 10^3$ [46]	$4.9(1) \times 10^4$ [47] $4.7(1) \times 10^4$ [45] $4.6(1) \times 10^4$ [48]
$^3P_2 - {}^1S_0$	M2	4.41×10^{-4} [38]	4.41×10^{-4} [38]	1.27×10^{-4} [38]			
$^3P_2 - {}^3P_1$	M1	9.12×10^{-7} [38]	1.60×10^{-5} [38]	8.26×10^{-4} [38]			
$^3P_2 - {}^3P_1$	E2	1.0×10^{-12} [38]	3.0×10^{-10} [38]	3.0×10^{-7} [38]			
$^3P_2 - {}^3P_0$	E2	3.0×10^{-12} [38]	1.0×10^{-9} [38]	1.0×10^{-6} [38]			
$^3P_0 - {}^1S_0$	E1 + M1	1.6×10^{-13} [39]	3.6×10^{-13} [39]	5.5×10^{-12} [39]			

Note that the value of A_{M1} estimated from (3) by using the experimental value of ω differs from the *ab initio* calculation [49] only by 3 %. The corrections of higher multiplicities for this transitions [related to the magnetic octupole (M3) decay channel and two-photon transition probability] are negligibly small, and can be neglected in the calculations of the total probability of transitions from the $^3P_2$ metastable level.

The numerical values of the magnetic quadrupole (M2) $^3P_2 - {}^1S_0$ transition probability were absent in the literature until recently. The only exclusion is the Mg atom for which the first estimates of the probability A_{M2} (1.6×10^{-4} s^{-1}) were obtained more than 30 years ago [50, 51]. The modern theoretical estimates are at least twice this value of A_{M2}, being well consistent with each other (4.44×10^{-4} s^{-1} [38] and 3.983×10^{-4} s^{-1} [49]). The probabilities of the electric quadrupole (E2) decay channel of the $^3P_2$ level to the $^3P_{0,1}$ levels are a few orders of magnitude lower than the probabilities of the M1 and M2 transitions (Table 2).

The one-photon transition from the $^3P_0$ level to the ground state is strictly forbidden by the selection rules for the atomic angular momentum, while the two-photon and three-photon transitions from this level are strongly suppressed (Table 2). However, in atoms with the nonzero nuclear spin (odd fermion isotopes of alkaline-earth atoms) the one-photon E1 transition to the ground state is possible, which is caused, on the one hand, by the singlet – singlet mixing of atomic levels of the same parity and the same total momenta and on the other, by the hyperfine interaction of the levels with the $^3P_1$ triplet level [39, 52 – 54]. As a result, for example, the radiative lifetime of the $^3P_0$ and $^3P_2$ levels can strongly decrease due to the additional E1 decay channel to the ground state induced by the hyperfine interaction (Table 3).

Table 3. Probabilities of the radiative decay of the metastable $^3P_0$ and $^3P_2$ levels induced by the hyperfine interaction in fermion isotopes of alkaline-earth atoms and in the Yb atom.

Atom	Transition	F	A_{ki}/s^{-1}	References
^{25}Mg	$^3P_0 - {}^1S_0$	5/2	4.44×10^{-4}	[52]
			4.2×10^{-4}	[55]
	$^3P_2 - {}^1S_0$	3/2	2.25×10^{-4}	[52]
			1.4×10^{-4}	[55]
	$^3P_2 - {}^1S_0$	5/2	4.65×10^{-4}	[52]
			2.9×10^{-4}	[55]
	$^3P_2 - {}^1S_0$	7/2	5.02×10^{-4}	[52]
			3.1×10^{-4}	[55]
^{43}Ca	$^3P_0 - {}^1S_0$	7/2	2.22×10^{-3}	[52]
	$^3P_2 - {}^1S_0$	5/2	1.02×10^{-3}	[52]
		7/2	1.81×10^{-3}	[52]
		9/2	1.74×10^{-3}	[52]
^{87}Sr	$^3P_0 - {}^1S_0$	9/2	7.58×10^{-3}	[52]
			6.3×10^{-3}	[29]
			5.5×10^{-3}	[56]
	$^3P_2 - {}^1S_0$	7/2	4.01×10^{-3}	[52]
		9/2	6.81×10^{-3}	[52]
		11/2	6.38×10^{-3}	[52]
^{171}Yb	$^3P_0 - {}^1S_0$	1/2	4.35×10^{-2}	[52]
			5.0×10^{-2}	[57]
	$^3P_2 - {}^1S_0$	3/2	9.18×10^{-2}	[52]
^{173}Yb	$^3P_0 - {}^1S_0$	5/2	3.85×10^{-2}	[52]
			4.3×10^{-2}	[57]

The numerical data presented in Tables 2 and 3 show that the lifetime $\tau = 1/A_{ki}$ of metastable levels of alkaline-earth atoms is $10^2 - 10^4$ s, while the typical natural widths of forbidden spectral lines do not exceed several millihertz. It is these unique radiative characteristics of forbidden transitions that stimulate wide applications of alkaline-earth atoms as working media in optical frequency standards.

3. Stark shift and splitting of atomic lines in a monochromatic field

To study the interaction of an atomic system with the field of a monochromatic wave

$$\boldsymbol{E}(\boldsymbol{r}, t) = E_0 \mathrm{Re}\{\boldsymbol{e} \exp[\mathrm{i}(\boldsymbol{k}\boldsymbol{r} - \omega t)]\} \tag{4}$$

(where E_0 and ω are the wave amplitude and frequency; $\boldsymbol{k} = \omega \boldsymbol{n}/c$ is the wave vector; $\boldsymbol{e}$ and $\boldsymbol{n}$ are the unit polarisation and wave-propagation vectors, respectively), it is convenient to use the concepts of quasi-energy and quasi-energy states [58 – 60]. In this case, the spectral characteristics of an atom in an external field are determined by the complex quasi-energies

$$\varepsilon = \mathrm{Re}\,\varepsilon - \mathrm{i}\Gamma/2, \tag{5}$$

with the imaginary and real parts corresponding to the Stark radiative-ionisation broadening Γ and the Stark shift

$$\Delta\varepsilon = \mathrm{Re}\,\varepsilon - E_{\beta J}^{(0)} \tag{6}$$

of the nondegenerate levels with energy $E_{\beta J}^{(0)}$ by the light-wave field (here, J is the total momentum and β is the set of quantum numbers). This approach allows one to solve most simply many problems of atomic and molecular spectroscopy, in particular, the problems of decay of weakly bound states [60 – 62] and a change in the atomic spectrum in a monochromatic field [60, 63, 64], and to study multiphoton processes [60] and the convergence of series in the perturbation theory for isolated and degenerate levels [64, 65], etc.

If the amplitude of monochromatic field (4) is small compared to the intra-atomic field amplitude $E_{at} \approx 5 \times 10^9$ V cm^{-1}, it is sufficient to use the lower-order corrections of the perturbation theory to calculate variations in the energy of an atom caused by the action of a light wave.

In the general case the shift $\Delta\varepsilon = \varepsilon - E_{\beta J}^{(0)}$ of quasi-energies of the $|\beta JM\rangle$ sublevels of an atomic multiplet with the projections M of the total momentum J caused by an external monochromatic field is determined from solutions of the secular equation [66, 67]

$$\det\|\Delta\varepsilon\delta_{J'J}\delta_{M'M} - U_{J'M'JM}\| = 0. \tag{7}$$

Therefore, the action of the electric field changes the spin–orbit structure of an atom, by mixing states with different total momenta J while the violation of the axial symmetry caused by the light wave leads to the mixing of the states with different magnetic quantum numbers M. As a result, the problem of the quasi-energy spectrum is reduced to the diagonalisation of a matrix in the subspace of closely spaced states of the multiplet with different momenta and different magnetic quantum numbers:

$$U_{J'M'JM} = -\langle\langle\, \beta J'M'|V(\boldsymbol{r},t)\mathcal{G}V(\boldsymbol{r},t)|\beta JM\,\rangle\rangle \tag{8}$$

(here, the double Dirac brackets denote integration with respect to coordinates and time averaging). The expression for the operator of interaction with an external field has the form

$$V(\boldsymbol{r},t) = v(\boldsymbol{r})\exp(-\mathrm{i}\omega t) + v^{+}(\boldsymbol{r})\exp(\mathrm{i}\omega t), \tag{9}$$

where

$$v(\boldsymbol{r}) = V_D + V_\mu + V_Q + ...; \tag{10}$$

$$V_D = -\frac{1}{2}\boldsymbol{DE} = \frac{E_0}{2}\boldsymbol{re}, \tag{11}$$

$$V_\mu = -\frac{1}{2}(\boldsymbol{\mu}[\boldsymbol{n}\times\boldsymbol{E}]) = \frac{\alpha E_0}{4}(\boldsymbol{J}+\boldsymbol{S})[\boldsymbol{n}\times\boldsymbol{e}], \tag{12}$$

$$V_Q = -\frac{\mathrm{i}}{6}\sum_{s_1,s_2} Q_{s_1,s_2}k_{s_1}E_{s_2}$$

$$= \frac{\mathrm{i}E_0\alpha\omega}{2\sqrt{6}}r^2\{\boldsymbol{n}\otimes\boldsymbol{e}\}_2 C_2(\theta,\varphi) \tag{13}$$

are the operators of electric dipole, magnetic dipole, and electric quadrupole interactions of an atom with the field, respectively [66]; in the one-electron approximation, $\boldsymbol{D} = -\boldsymbol{r}$, $\boldsymbol{\mu} = -\alpha(\boldsymbol{J}+\boldsymbol{S})/2$ and $Q = -r^2C_2(\theta,\varphi)$ are the electric dipole, magnetic dipole, and electric quadrupole momenta of an atom, respectively; and $C_2(\theta,\varphi)$ is the modified spherical function of the angular variables of the radius vector $\boldsymbol{r}$ of a valence electron. In expression (8),

$$\mathcal{G}(\boldsymbol{r},t;\boldsymbol{r}'t') = \sum_{m,\kappa}\frac{\langle\langle \boldsymbol{r},t|m,\kappa\rangle\rangle\langle\langle m,\kappa|\boldsymbol{r}',t'\rangle\rangle}{\varepsilon_{m\kappa}-E_{\beta J}} \tag{14}$$

is the reduced quasi-energy Green function expanded in the quasi-energy states $\langle\langle \boldsymbol{r},t|m,\kappa\rangle\rangle = \langle\boldsymbol{r}|m\rangle\exp(\mathrm{i}\kappa\omega t)$ of an unperturbed atom with the quasi-energy $\varepsilon_{m\kappa} = E_m + \kappa\omega$. The time dependence of the Green function (14) can be separated explicitly in the form of the Fourier expansion [66]

$$\mathcal{G}(\boldsymbol{r},t;\boldsymbol{r}'t') = \sum_{\kappa} G^{E_{\beta J}-\kappa\omega}(\boldsymbol{r};\boldsymbol{r}')\exp[\mathrm{i}\kappa\omega(t-t')], \tag{15}$$

the coefficients of which are stationary Green's functions

$$G^{(\varepsilon)}(\boldsymbol{r};\boldsymbol{r}') = \sum_m \frac{\langle\boldsymbol{r}|m\rangle\langle m|\boldsymbol{r}'\rangle}{E_m-\varepsilon}, \tag{16}$$

where summation is performed over a complete set of states except the initial state $|m\rangle = |\beta JM\rangle$ ($M = 0, \pm1, ..., \pm J$).

After time averaging and integration with respect to the angular variables, matrix element (8) can be written in the form of expansion in the irreducible tensor products $\{\boldsymbol{e}\otimes\boldsymbol{e}^*\}_{j\chi}$ of the polarisation vector $\boldsymbol{e}$ and its complex conjugate vector $\boldsymbol{e}^*$ of ranks $j = 0, 1, 2$ (expansion in the components of the polarisation tensor [66, 67]):

$$U_{J'M'JM} = \frac{E_0^2}{2}w_{J'M'JM}, \tag{17}$$

where

$$w_{J'M'JM} = -\frac{1}{2}\langle\beta J'M'|\boldsymbol{e}^*\boldsymbol{r}'\,G^{E_{\beta J}+\omega}(\boldsymbol{r};\boldsymbol{r}')\boldsymbol{e}\boldsymbol{r}'$$

$$+\boldsymbol{e}\boldsymbol{r}\,G^{E_{\beta J}-\omega}(\boldsymbol{r};\boldsymbol{r}')\boldsymbol{e}^*\boldsymbol{r}'|\beta JM\,\rangle$$

$$= -\frac{1}{2}\sum_{\chi,j=0,1,2}(-1)^{\chi}C^{J'M'}_{JMj-\chi}b^{(j)}_{J'J}\{\boldsymbol{e}\otimes\boldsymbol{e}^*\}_{j\chi}. \tag{18}$$

The factor $-1/2$ in front of the sum of second-order matrix elements is retained here to provide the coincidence of the values of the matrix element $w_{J'M'JM}$ in the static limit ($\omega = 0$) with analogous values introduced in [68] for the stationary Stark effect on the triplet levels of He. Expansion coefficients (18) are represented as products of the Clebsch–Gordan coefficients $C^{J'M'}_{JMj-\chi}$ and irreducible atomic parameters

$$b^{(j)}_{J'J} = (-1)^{J'+J+j}\left(\frac{2j+1}{2J'+1}\right)^{1/2}\sum_{J_1}\begin{Bmatrix} 1 & 1 & j \\ J' & J & J_1\end{Bmatrix}$$

$$\times[R_{J_1}(\omega) + (-1)^j R_{J_1}(-\omega)], \tag{19}$$

where

$$\begin{Bmatrix} 1 & 1 & j \\ J' & J & J_1\end{Bmatrix}$$

is the standard notation of the $6j$ symbol;

$$R_{J_1}(\omega) = \langle\beta J'\|\boldsymbol{D}G^{E_{\beta J}+\omega}_{J_1}\boldsymbol{D}\|\beta J\rangle \tag{20}$$

is the reduced second-order dipole matrix element with the partial Green function from the subspace of stages with a fixed value of the total momentum J_1. The further integration over the angular variables allows us to express the reduced matrix element (20) in terms of a superposition of radial matrix elements, which depend on the specific spin–orbit structure of intermediate states. In a particular case of the LS coupling scheme, a set of quantum numbers β consists of the principal (n), orbital (L), and spin (S) quantum numbers: $\beta = \{nLS\}$. After the calculation of reduced matrix elements of the dipole moment in the LS coupling scheme, expression (19) takes the form

$$b^{(j)}_{J'J} = (2L+1)[(2J+1)(2j+1)]^{1/2}$$

$$\times\sum_{L_1,J_1}(-1)^{J'+J_1+j}(2J_1+1)\times$$

$$\times (C^{L_1 0}_{L010})^2 \begin{Bmatrix} 1 & 1 & j \\ J' & J & J_1 \end{Bmatrix} \begin{Bmatrix} L_1 & S & J_1 \\ J' & 1 & L \end{Bmatrix} \begin{Bmatrix} 1 & J & J_1 \\ S & L_1 & L \end{Bmatrix} \sigma^{(j)}_{L_1 J_1}(\omega), \quad (21)$$

where

$$\sigma^{(j)}_{L_1 J_1}(\omega) = \langle nLSJ' | r \Big[g^{E^{(0)}_{nLSJ}+\omega}_{L_1 J_1}(r, r') + (-1)^j g^{E^{(0)}_{nLSJ}-\omega}_{L_1 J_1}(r, r') \Big] r' | nLSJ \rangle \quad (j = 0, 1, 2) \quad (22)$$

is the sum (for $j = 0,\ 2$) or difference (for $j = 1$) of the second-order radial matrix elements with the positive-frequency $[g^{E^{(0)}_{nLSJ}+\omega}_{L_1 J_1}(r, r')]$ and negative-frequency $[g^{E^{(0)}_{nLSJ}-\omega}_{L_1 J_1}(r, r')]$ radial Green functions in the subspace of states with fixed orbital and total momenta L_1 and J_1 (the spin moment S remains invariable in electric dipole transitions).

Expression (21) is considerably simplified if the radial matrix elements (22) for a fixed orbital momentum L_1 are independent of the total momentum J_1, i.e., if the influence of the spin–orbit splitting of levels on matrix elements can be neglected, by writing $\sigma^{(j)}_{L_1 J_1}(\omega) \equiv \sigma^{(j)}_{L_1}(\omega)$. Then, summation over J_1 in (21) can be performed analytically:

$$b^{(j)}_{J'J} = (-1)^{1+L+S+J}(2L+1)[(2J+1)(2j+1)]^{1/2} \times \begin{Bmatrix} L & L & j \\ J' & J & S \end{Bmatrix} \sum_{L_1} (C^{L_1 0}_{L010})^2 \begin{Bmatrix} 1 & 1 & j \\ L & L & L_1 \end{Bmatrix} \sigma^{(j)}_{L_1}(\omega). \quad (23)$$

In this approximation, all matrix elements (17) can be expressed in terms of three independent components of the tensor of dynamic polarisability of the $|nLSJ\rangle$ state.

The components of polarisation tensor (18) depend on the polarisation type of the radiation field (4). Assuming the wave completely polarised, we consider the most general case of elliptic polarisation. The field of such a wave has two selected directions: the wave propagation direction, which is specified by the unit wave vector $\boldsymbol{n} = (\lambda/2\pi)\boldsymbol{k}$, and the direction of the principal axis of the polarisation ellipse, which is specified by the vector $\boldsymbol{u}$ perpendicular to $\boldsymbol{n}$. It is convenient to introduce the orthogonal basis of the unit vectors $\boldsymbol{e}_z = \boldsymbol{n}$, $\boldsymbol{e}_x = \boldsymbol{u}$, and $\boldsymbol{e}_y = \boldsymbol{n} \times \boldsymbol{u}$. Then, the unit polarisation vector in (4) can be written in the form

$$\boldsymbol{e} = \frac{\boldsymbol{e}_x + \mathrm{i}\gamma \boldsymbol{e}_y}{(1+\gamma^2)^{1/2}}, \quad (24)$$

where γ is the ellipticity parameter ($-1 \leqslant \gamma \leqslant 1$) determining the degrees of linear polarisation $l = (1-\gamma^2)/(1+\gamma^2)$ ($0 \leqslant l \leqslant 1$) and circular polarisation $\xi = 2\gamma/(1+\gamma^2)$ ($-1 \leqslant \xi \leqslant 1$), and $l^2 + \xi^2 = 1$ according to the condition of 100 % polarisation of radiation. By expanding vector (24) in the cyclic basis of vectors [69] $\boldsymbol{e} = (\boldsymbol{e})_i \boldsymbol{e}^i$, where $i = 0, \pm 1$, $\boldsymbol{e}^0 = \boldsymbol{e}_z$, $\boldsymbol{e}^{\pm 1} = \mp(\boldsymbol{e}_x \mp \mathrm{i}\boldsymbol{e}_y)/\sqrt{2}$, we obtain the expressions

$$(\boldsymbol{e})_0 = 0, \quad (\boldsymbol{e})_{\pm 1} = -(\boldsymbol{e}^*)_{\mp 1} = \mp \frac{1 \mp \gamma}{[2(1+\gamma^2)]^{1/2}} \quad (25)$$

for cyclic components. The parameter χ of the polarisation tensor in (18) in the coordinate system specified in this way can take values 0 and ± 2, i.e., only five components from the nine tensor components $\{\boldsymbol{e} \otimes \boldsymbol{e}^*\}_{j\chi}$ can be nonzero. They can be written in the form

$$\{\boldsymbol{e} \otimes \boldsymbol{e}^*\}_{j\chi} = -\xi^{\delta_{j1}} C^{j0}_{1-111} \delta_{\chi 0} + \frac{l}{2}\delta_{j2}(\delta_{\chi 2} + \delta_{\chi -2}) = \left(-\frac{1}{\sqrt{3}}\delta_{j0} + \frac{\xi}{\sqrt{2}}\delta_{j1} - \frac{1}{\sqrt{6}}\delta_{j2} \right)\delta_{\chi 0} + \frac{l}{2}\delta_{j2}(\delta_{\chi 2} + \delta_{\chi -2}). \quad (26)$$

Therefore, matrix (18) is completely determined by the set of invariant atomic parameters (21):

$$w_{J'M'JM} = -\frac{1}{2}\delta_{M'M}\left(-\frac{b^{(0)}_{JJ}}{\sqrt{3}}\delta_{J'J} + \xi\frac{b^{(1)}_{J'J}}{\sqrt{2}} C^{J'M}_{JM10} - \frac{b^{(2)}_{J'J}}{\sqrt{6}} C^{J'M}_{JM20} \right) - \frac{l}{4} b^{(2)}_{J'J}(C^{J'M'}_{JM2-2} + C^{J'M'}_{JM22}). \quad (27)$$

Each of these parameters can be expressed in approximation (23) in terms of three independent characteristics of the multiplet – the components of the polarisability tensor [66, 67, 70–72]. Thus, the quantity $b^{(0)}_{JJ}$, contributing only to the diagonal matrix element ($J' = J$, $M' = M$) (27) can be written in the form

$$b^{(0)}_{JJ} = -\sqrt{3}\alpha^{\mathrm{s}}_{nLJ}(\omega), \quad (28)$$

where

$$\alpha^{\mathrm{s}}_{nLJ}(\omega) = \frac{1}{3(2J+1)} \sum_{J_1 = J, J\pm 1} (-1)^{J_1 - J}[R_{J_1}(\omega) + R_{J_1}(-\omega)] \quad (29)$$

is the scalar polarisability, which is the same for all the sublevels of the multiplet in approximation (23), i.e., is independent of the total momentum J:

$$\alpha^{\mathrm{s}}_{nLJ}(\omega) \approx \alpha^{\mathrm{s}}_{nL}(\omega) = \frac{1}{3(2L+1)} \times [L\sigma^{+}_{L-1}(\omega) + (L+1)\sigma^{+}_{L+1}(\omega)] \quad (30)$$

[hereafter, we use the notation $\sigma^{(0)}_{L_1}(\omega) = \sigma^{(2)}_{L_1}(\omega) \equiv \sigma^{+}_{L_1}(\omega)$, $\sigma^{(1)}_{L_1}(\omega) \equiv \sigma^{-}_{L_1}(\omega)$]. By using (23), the quantities $b^{(1)}_{J'J}$ contributing to matrix elements (27) with $J' = J, J \pm 1$, $M' = M$, can be also expressed in terms of the diagonal component $b^{(1)}_{JJ}$:

$$b^{(1)}_{J'J} = b^{(1)}_{JJ} \begin{Bmatrix} L & L & 1 \\ J' & J & S \end{Bmatrix} \Big/ \begin{Bmatrix} L & L & 1 \\ J & J & S \end{Bmatrix}, \quad (31)$$

which in turn is expressed in terms of the antisymmetric (vector or axial) polarisability:

$$b^{(1)}_{JJ} = \alpha^{\mathrm{a}}_{nLSJ}\left(\frac{J+1}{2J}\right)^{1/2}, \quad \alpha^{\mathrm{a}}_{nLSJ} = \frac{1}{(2J+1)_2} \times \sum_{J_1 = J, J\pm 1} (-1)^{J_1 - J} X [R_{J_1}(\omega) - R_{J_1}(-\omega)], \quad (32)$$

where $X = J(J+1) + 2 - J_1(J_1+1)$ and the conventional notation $(x)_n = x(x+1)...(x+n-1)$ for the Pochhammer symbol [73] is used. In this case, the dependence on the total momentum can be also written explicitly:

$$\alpha^{\rm a}_{nLSJ} \approx (-1)^{J+L+S+1}\left[\frac{(2L+1)_2(2J)_2}{4L(J+1)}\right]^{1/2}\left\{\begin{matrix} S & L & J \\ 1 & J & L \end{matrix}\right\}\alpha^{\rm a}_{nL}$$

$$= \frac{Y}{2L(J+1)}\alpha^{\rm a}_{nL}, \qquad (33)$$

where $Y = J(J+1) + L(L+1) - S(S+1)$;

$$\alpha^{\rm a}_{nL} = \frac{L}{(2L+1)}[\sigma^{-}_{L-1}(\omega) - \sigma^{-}_{L+1}(\omega)] \qquad (34)$$

is the characteristic which is the same for all the sublevels and coincides with the axial polarisability of the state with the maximum total momentum $J = L + S$.

The quantities $b^{(2)}_{J'J}$ make a contribution to matrix elements (27) with $J' = J, J \pm 1, J \pm 2$ and $M' = M$, $M \pm 2$. They can be expressed in terms of the symmetric (or tensor) polarisability

$$b^{(2)}_{J'J} = b^{(2)}_{JJ}\left\{\begin{matrix} L & L & 2 \\ J' & J & S \end{matrix}\right\}\Big/\left\{\begin{matrix} L & L & 2 \\ J & J & S \end{matrix}\right\},$$

$$b^{(2)}_{JJ} = \alpha^{\rm t}_{nLSJ}\left[\frac{3(2J+2)_2}{2(2J-1)_2}\right]^{1/2}, \qquad (35)$$

where

$$\alpha^{\rm t}_{nLSJ} = -\frac{1}{3(2J+1)_3}\sum_{J_1=J,\,J\pm1}(-1)^{J_1-J}$$

$$\times[3X(X-1) - 8J(J+1)]\,[R_{J_1}(\omega) + R_{J_1}(-\omega)]. \qquad (36)$$

Similarly to (33), we can write

$$\alpha^{\rm t}_{nLSJ} \approx (-1)^{J+L+S}\left[\frac{(2L+1)_3(2J-1)_3}{(2L-1)_2(2J+2)_2}\right]^{1/2}\left\{\begin{matrix} S & L & J \\ 2 & J & L \end{matrix}\right\}\alpha^{\rm t}_{nL}$$

$$= 2\frac{3Y(Y-1) - 4L(L+1)J(J+1)}{(2L-1)_2(2J+2)_2}\alpha^{\rm t}_{nL}, \qquad (37)$$

where

$$\alpha^{\rm t}_{nL} = -\frac{L}{3(2L+1)}\left[\sigma^{+}_{L-1}(\omega) + \frac{2L-1}{2L+3}\sigma^{+}_{L+1}(\omega)\right] \qquad (38)$$

is the characteristic that is common for all the sublevels of the multiplet and coincides with the tensor polarisability of the sublevel with the total momentum $J = L + S$.

Therefore, by using polarisabilities (30), (34), and (38), we can represent the general expression for matrix element (27) in the form

$$w_{J'M'JM} = -\frac{1}{2}\Bigg\{\alpha^{\rm s}_{nL}\delta_{J'J} + \frac{\xi}{2}(-1)^{L+S+J+1}C^{J'M}_{JM10}$$

$$\times\left[\frac{(2L+1)_2(2J+1)}{2L}\right]^{1/2}\left\{\begin{matrix} S & L & J \\ 1 & J' & L \end{matrix}\right\}\alpha^{\rm a}_{nL}\Bigg\}\delta_{M'M}$$

$$+\frac{(-1)^{L+S+J}}{4}\left[\frac{(2L+1)_3(2J+1)}{(2L-1)_2}\right]^{1/2}\left\{\begin{matrix} S & L & J \\ 2 & J' & L \end{matrix}\right\}\alpha^{\rm t}_{nL}\times$$

$$\times\left[\delta_{M'M}C^{J'M}_{JM20} - l\left(\frac{3}{2}\right)^{1/2}(C^{J'M'}_{JM2-2} + C^{J'M'}_{JM22})\right]. \qquad (39)$$

If the energy of interaction of an atom with an external field is much lower than the spin–orbit splitting, the influence of nondiagonal (in J) matrix elements can be neglected. In a circularly polarised field ($\xi = \pm1$, $l = 0$), matrix (39) becomes also diagonal in M, i.e., the projection of the total momentum on the wave propagation direction is the integral of motion. In this case, the diagonal matrix element

$$w_{JMJM} = -\frac{1}{2}\left[\alpha^{\rm s}_{nL} + \frac{M}{2J}\xi\alpha^{\rm a}_{nLSJ} - \frac{3M^2 - J(J+1)}{2J(2J-1)}\alpha^{\rm t}_{nLSJ}\right] \qquad (40)$$

completely determines the shift and splitting (in the momentum projections) of the quasi-energy of the isolated $|nLSJ\rangle$ state. If $l \neq 0$, the magnetic quantum number is no longer the integral of motion, while the nondiagonal (in M) matrix element

$$w_{JM\pm2JM} = -\frac{3l[(J \pm M + 1)_2(J \mp M - 1)_2]^{1/2}}{4(2J-1)_2}\alpha^{\rm t}_{nLSJ} \qquad (41)$$

determines the relative contribution of the states with momentum projections $M' = M \pm 2$ to the state with the projection M. The quasi-energy value is found by diagonalising the matrix with elements (40) and (41).

Consider as an example the $n{\rm P}_1$ state in an elliptically polarised field. In this case, matrix elements (40) and (41) take the form

$$w_{1\pm1\,1\pm1} = -\frac{1}{2}\left(\alpha^{\rm s}_{n{\rm P}} \pm \frac{1}{2}\xi\alpha^{\rm a}_{n{\rm P}_1} - \frac{1}{2}\alpha^{\rm t}_{n{\rm P}_1}\right),$$

$$w_{10\,10} = -\frac{1}{2}\left(\alpha^{\rm s}_{n{\rm P}} + \alpha^{\rm t}_{n{\rm P}_1}\right),$$

$$w_{1-1\,11} = w_{11\,1-1} = -\frac{3l}{4}\alpha^{\rm t}_{n{\rm P}_1}.$$

Secular equation (7) with these matrix elements gives the three solutions

$$\Delta\varepsilon_{\pm} = -\frac{E_0^2}{4}\Bigg\{\alpha^{\rm s}_{n{\rm P}} - \frac{\alpha^{\rm t}_{n{\rm P}_1}}{2} \pm \frac{3}{2}\alpha^{\rm t}_{n{\rm P}_1}$$

$$\times\left\{1 + \xi^2\left[\left(\frac{\alpha^{\rm a}_{n{\rm P}_1}}{\alpha^{\rm t}_{n{\rm P}_1}}\right)^2 - 1\right]\right\}^{1/2}\Bigg\}, \qquad (42)$$

$$\Delta\varepsilon_0 = -\frac{E_0^2}{4}(\alpha^{\rm s}_{nP} + \alpha^{\rm t}_{n{\rm P}_1}).$$

For linearly polarised radiation ($l = 1$, $\xi = 0$), the dependence of these solutions on the axial polarisability $\alpha^{\rm a}_{n{\rm P}_1}$ disappears and $\Delta\varepsilon_+ = \Delta\varepsilon_0$, which corresponds to the degeneracy over the sign of the momentum projection on the direction of the polarisation vector $\boldsymbol{e} = \boldsymbol{e}^* = \boldsymbol{e}_x$. In the case of circular polarisation ($\xi = \pm1$, $l = 0$), nondiagonal matrix elements (41) vanish and then three values of the quasi-energy shift are determined by three diagonal elements $w_{1M\,1M}$ ($M = 0, \pm1$).

Therefore, the calculation of the quasi-energy of an atom in a field in the approximation quadratic in the radiation

field strength is reduced to the calculation of three independent quantities – components of the polarisability tensor of the multiplet under study. Finally, these quantities are determined by the second-order radial dipole matrix elements, which can be written in terms of the spectral sum of the oscillator strengths of radiative transitions described by the expression [35]

$$f(\beta_1 J_1;\beta J)=\frac{1}{2J+1}\sum_{M_1,M}2(E_{\beta_1 J_1}-E_{\beta J})$$

$$\times|\langle\beta_1 J_1 M_1|\boldsymbol{D}|\beta J M\rangle|^2=\frac{2(E_{\beta_1 J_1}-E_{\beta J})}{3(2J+1)}|\langle\beta_1 J_1\|\boldsymbol{D}\|\beta J\rangle|^2.$$

Then

$$\alpha^{\mathrm{s}}(\omega)=\sum_{\beta_1,J_1}\frac{f(\beta_1 J_1;\beta J)}{\left[\left(E^{(0)}_{\beta_1 J_1}-E^{(0)}_{\beta J}\right)^2-\omega^2\right]}, \tag{43}$$

$$\alpha^{\mathrm{a}}(\omega)=-\frac{3\omega}{2(J+1)}\sum_{\beta_1,J_1}\frac{X}{\left(E^{(0)}_{\beta_1 J_1}-E^{(0)}_{\beta J}\right)}$$

$$\times\frac{f(\beta_1 J_1;\beta J)}{\left[\left(E^{(0)}_{\beta_1 J_1}-E^{(0)}_{\beta J}\right)^2-\omega^2\right]}, \tag{44}$$

$$\alpha^{\mathrm{t}}(\omega)=-\sum_{\beta_1,J_1}\frac{3X(X-1)-8J(J+1)}{(2J+2)_2}$$

$$\times\frac{f(\beta_1 J_1;\beta J)}{\left[\left(E^{(0)}_{\beta_1 J_1}-E^{(0)}_{\beta J}\right)^2-\omega^2\right]}. \tag{45}$$

Note that the tensor polarisability in a constant field determines the main (resonance) part of the fourth-order correction to the sublevel energy [66, 74, 75].

If the separation of the interaction sublevels considerably exceeds a change in the quasi-energy of the atom and the magnetic quantum number remains the integral of motion, it is sufficient to use the perturbation theory for nondegenerate states for calculating the field corrections. In this case, the change in the energy ΔE of the isolated state $|\beta JM\rangle$ of an atom caused by the light-wave field (4) in the quadratic approximation (over the field strength) also can be analysed with the help of the dynamic polarisability $\alpha(\boldsymbol{e},\omega)$, and in the fourth-order approximation – by using the dynamic hyperpolarisability $\gamma(\boldsymbol{e},\omega)$:

$$\Delta E=E-E^{(0)}=\Delta E^{(2)}+\Delta E^{(4)}+\dots, \tag{46}$$

$$\Delta E^{(2)}=-\frac{1}{4}\alpha_{\beta JM}(\boldsymbol{e},\omega)E_0^2=-\langle\langle\beta JM|VGV|\beta JM\rangle\rangle, \tag{47}$$

$$\Delta E^{(4)}=-\frac{1}{64}\gamma_{\beta JM}(\boldsymbol{e},\omega)E_0^4$$

$$=-\langle\langle\beta JM|VGVGVGV|\beta JM\rangle\rangle+\langle\langle\beta JM|VGV|\beta JM\rangle\rangle$$

$$\times\langle\langle\beta JM|VG^2V|\beta JM\rangle\rangle. \tag{48}$$

The dynamic susceptibilities of the second and fourth orders $\alpha_{\beta JM}$ and $\gamma_{\beta JM}$ in (47) and (48) also determine the external-field-induced dipole moment of the atom at the frequency ω with an accuracy of the third-order terms [65]:

$$D_j(\omega,t)=\mathrm{Re}[\,D_j^{(\omega)}\exp(-\mathrm{i}\omega t)+D_j^{(3\omega)}\exp(-3\mathrm{i}\omega t)+\dots],$$

$$D_j^{(\omega)}=\alpha_{jk}e_k E_0+\frac{1}{16}\gamma_{jklm}e_k^* e_l e_m E_0^3. \tag{49}$$

According to definitions (47) and (48), the transition frequency in an atom in an alternating external field is described by the expression [60]

$$\omega_{\mathrm{fi}}=\omega_{\mathrm{fi}}^{(0)}-\frac{E_0^2}{4}\Delta\alpha(\boldsymbol{e},\omega)-\frac{E_0^4}{64}\Delta\gamma(\boldsymbol{e},\omega)-\dots, \tag{50}$$

in which $\omega_{\mathrm{fi}}^{(0)}$ corresponds to the unperturbed transition frequency in the absence of the field, and $\Delta\alpha(\boldsymbol{e},\omega)$ and $\Delta\gamma(\boldsymbol{e},\omega)$ are the differences of dynamic polarisabilities and hyperpolarisabilities of the initial ($|\mathrm{i}\rangle$) and final ($|\mathrm{f}\rangle$) states.

For atoms with the nonzero nuclear moment I, for example, fermion isotopes of alkaline-earth atoms, the quadratic Stark effect is described by similar expressions (for simplicity, we consider the case of a linearly polarised field acting on the atomic level $|\beta JFM_F\rangle$):

$$\Delta E^{(2)}=-\frac{E_0^2}{4}\left[\alpha_F^{\mathrm{s}}(\omega)+\alpha_F^{\mathrm{t}}(\omega)\frac{3M_F^2-F(F+1)}{F(2F-1)}\right]. \tag{51}$$

Here, F is the total momentum of the atom taking the hyperfine structure into account. By assuming that the hyperfine interaction does not affect substantially the electronic part of the wave function (the IJ-coupling approximation [70]), we obtain that the scalar and tensor components of the polarisability of the $|\beta JFM_F\rangle$ level are related to $\alpha^{\mathrm{s}}_{nLSJ}(\omega)$ and $\alpha^{\mathrm{t}}_{nLSJ}(\omega)$ in (51) by simple expressions

$$\alpha_F^{\mathrm{s}}(\omega)=\alpha_{nL}^{\mathrm{s}}(\omega),$$

$$\alpha_F^{\mathrm{t}}(\omega)=(-1)^{I+J+F}$$

$$\times\left[\frac{F(2F-1)(2F+1)(2J+3)(2J+1)(J+1)}{(2F+3)(F+1)J(2J-1)}\right]^{1/2}$$

$$\times\left\{\begin{array}{ccc}F & J & I\\ J & F & 2\end{array}\right\}\alpha^{\mathrm{t}}_{nLSJ}(\omega)$$

$$=\frac{3Y_F(Y_F-1)-4J(J+1)F(F+1)}{(2F+2)_2(2J-1)_2}\alpha^{\mathrm{t}}_{nLSJ}(\omega),$$

where

$$Y_F=F(F+1)+J(J+1)-I(I+1). \tag{52}$$

However, the theoretical calculations of the shift and Zeeman splitting of the transition between the hyperfine-structure levels of the states with zero orbital and (or) total momenta (in particular, the ground states of atoms) in constant and alternating electromagnetic fields are complicated by the necessity of calculating the matrix elements of the third-order perturbation theory, which contain two

Green functions and the operator of hyperfine interaction between the electron shell and atomic nucleus [76–79].

Expressions similar to (51) and (52) can be also written for the irreducible components of the dynamic hyperpolarisability (fourth-rank tensor); however, they are too cumbersome [66, 67, 74] to be presented here.

4. Choice of the basis wave functions in light-shift calculations for alkaline-earth atoms

At present the most precise calculations of the spectral characteristics of alkaline-earth atoms were performed within the framework of the many-particle perturbation theory, in which the effects of configuration interaction were taken consistently into account [37, 38, 40, 49, 57]. In this approach, the energies $E_{\beta J}$ and eigenfunctions $|\Psi_{\beta J}\rangle$ were determined by solving the wave equation

$$H_{\rm eff}(E_{\beta J})|\Psi_{\beta JM}\rangle = E_{\beta J}|\Psi_{\beta JM}\rangle, \tag{53}$$

in which the effective Hamiltonian was written in the form

$$H_{\rm eff}(E_n) = H_{\rm fc} + \Sigma. \tag{54}$$

Here, $H_{\rm fc}$ is the two-electron Hamiltonian in the frozen atomic core approximation and Σ are corrections to $H_{\rm fc}$ taking into account the interaction of valence electrons with electrons of the atomic core. In the frozen core approximation, the wave vector $|\Psi_{\beta JM}\rangle$ is written in the form of expansion in the two-particle basis functions $|\Phi_q\rangle \equiv |\Phi_{JM}(ij)\rangle$:

$$|\Psi_{\beta JM}\rangle = \sum_q C_q|\Phi_q\rangle, \tag{55}$$

where the total angular momentum J, the projections M and parities are fixed. The weight coefficients C_q normalised by the condition

$$\sum_q |C_q|^2 = 1 \tag{56}$$

are determined from the variation principle by using the relativistic Hamiltonian

$$\langle\Psi_{\beta JM}|H_{\rm fc}|\Psi_{\beta JM}\rangle = \sum_q E_q C_q^2 + \sum_{q,p} V_{qp} C_q C_p \tag{57}$$

averaged by expression (55), which includes the Coulomb and Breit electron–electron interaction operators. In (57), $E_q = E_i + E_j$ is the sum of one-particle Dirac–Fock energies and V_{qp} is the first-order matrix element for two-particle interactions between configurations $q = (ij)$ and $p = (kl)$. The energy E and the wave function $\sum_q C_q|\Phi_q\rangle$ are determined by the solutions of the system of equations [37]

$$\sum_p (E_q\delta_{qp} + V_{qp})C_p = EC_q. \tag{58}$$

One-particle basis orbitals used to construct the two-particle basis functions $|\Phi_q\rangle$ in (55) include the partial s, p, d, f, and g waves with the spline approximation of each of them. The estimates of the divergence rate of the method (for the specified accuracy) are described in [80, 81]. The most complex component of the configuration interaction method is the consideration of the correction Σ in Hamiltonian (54), which describes the interaction of the core and valence electrons and the polarisation of the atomic core by valence electrons. This consideration is performed within the framework of the many-particle lowest-order perturbation theory [37].

The calculations of spectral characteristics of alkaline-earth atoms by the method described above are, as a rule, quite complicated and time-consuming even when modern highly efficient computers are used. In addition, as follows from calculations, the technical problems of this method significantly increase when the higher-order effects (over an external electromagnetic field) of the perturbation theory should be estimated. This circumstance stimulates the development of approximate, less rigorous semiempirical calculation methods, which use the spectral characteristics of atoms obtained either from experiments or within the framework of other, more accurate theoretical methods. The calculation formula used in these methods are rather simple and clear, and contain a comparatively small number of free semiempirical parameters, which weakly depend on the energy, nucleus charge or quantum numbers of the atomic levels under study.

In this paper, we calculated numerically the second- and fourth-order dynamic susceptibilities by the model potential method in which the role of basis wave functions was limited mainly by the description of the optical properties of valence electrons, while their interaction with the atomic core was considered phenomenologically by introducing the effective potential [82]. Various modifications of the model potential method and its validity for calculating the spectra and probabilities of radiative transitions in alkaline-earth atoms are considered, for example, in papers [39, 83–89]. In this paper, we used Fues' potential [87] whose efficiency is determined to a considerable degree by the possibility of obtaining closed analytic expressions for the wave functions and the Green function of valence electrons in the calculations of matrix elements in arbitrary orders of the perturbation theory [66]. The Fues' model potential is described by the expression [87–89]

$$U_{\rm F}(r) = -\frac{Z}{r} + \sum_L \frac{B_L}{r^2}\hat{P}_L, \tag{59}$$

where Z is the residual ion charge and $\hat{P}_L$ is the operator of projection on the subspace of spherical functions with the given orbital momentum L. The parameters B_L of the potential are determined from the conditions of coincidence of the experimental value of the lower-level energy with a given L with the corresponding eigenvalue of the Hamiltonian. Therefore, Fues' model potential is described by a continuous function for which the analytic solution of the Schrödinger equation exists. This circumstance is quite important because the Green functions in the theory of a multielectron atom can be constructed only by approximate methods whose choice depends first of all on the problem type and the accuracy required for measuring the energy spectrum (poles of the Green function) and wave functions (residues in the poles).

The Green function for the Fues model potential (59) is constructed similarly to the Green function for a Coulomb field by using the expansion in the Sturm functions. For example, the expression for the radial part of the Green function of the model potential has the form [66]

$$g_L(E;r_1,r_2)=\frac{4Z}{\nu}$$

$$\times\sum_{k=0}^{\infty}\frac{k!\exp[-(x_1+x_2)/2](x_1x_2)^{\lambda_L}L_k^{2\lambda_L+1}(x_1)L_k^{2\lambda_L+1}(x_2)}{\Gamma(k+2+2\lambda_L)(k+\lambda_L+1-\nu)}. \quad (60)$$

Here, $x_j=2Zr_j/\nu$ $(j=1,2)$; $\nu=Z/(-2E-\mathrm{i}0)^{1/2}$; $L_k^m(x)$ is the Laguerre polynomial; and $\Gamma(x)$ is the Euler gamma function. The radial wave functions for the coupled states of the atom are obtained from the residues of the radial Green function (60) in poles determined by the expression $n_\mathrm{r}+\lambda_L+1-\nu_{nL}=0$, where $n_\mathrm{r}=0,1,2,...$ is the radial quantum number; λ_L is the effective orbital momentum; and ν_{nL} is the effective principal quantum number in the expression for the energy of the atomic $|nL\rangle$ state

$$E_{nL}=-\frac{Z^2}{2\nu_{nL}^2}. \quad (61)$$

The parameter λ_L is determined from the condition of coincidence of (61) with the experimental energy of the lower state of a valence electron with a given L [89, 90]. Note here that the absolute convergence of series of Laguerre polynomials (60) takes place only for negative energy parameters providing the real value of ν. However, for frequencies above the threshold, at which the energies of the Green function become positive, the convergence of series (60) is violated, which requires the use of the generalised Sturm expansion (for the Coulomb potential, see, for example, [91–93]) to obtain the universal closed expressions for combined matrix elements. The spectral expansion of the general form

$$g_L(E;r_1,r_2)=\sum_n{}'\frac{R_{nL}(r_1)R_{nL}(r_2)}{E_n-E}$$

$$+\int_0^\infty \mathrm{d}\varepsilon\frac{R_{\varepsilon L}(r_1)R_{\varepsilon L}(r_2)}{\varepsilon-E-\mathrm{i}0} \quad (62)$$

is useful only for analysis of the structure of radial matrix elements, in particular, for the estimate of the high-frequency asymptotics, the separation of the real and imaginary parts in the transition amplitudes, etc. However, the application of this representation for the numerical calculation of matrix elements, especially in the high orders of the perturbation theory, becomes quite problematic due to the necessity of calculations of integrals over the continuous-spectrum states and a weak convergence of series in the discrete-spectrum states. In addition, triple and multiple series over the discrete spectrum diverge [91], i.e., spectral expansion (62) cannot be used for calculating fourth-order corrections.

We formulated [75, 94, 95] a modified variant of the Fues model potential theory, which allowed us to calculate more accurately the spectroscopic characteristics of atoms in the ground and highly excited states of a valence electron. Thus, the wave function for alkali atoms coincides with the wave function of the quantum defect theory [96] if the radial quantum number for the ground state is set equal to unity and the effective orbital momentum λ_L is set equal to $\nu_\mathrm{g}-2$ (ν_g is the effective principal quantum number of the ground state). For the values of λ_L and n_r chosen in this way, the wave function of the atom is multiplied by the additional phase factor $(-1)^i$, where $i=n-n_\mathrm{r}-1$. It was shown in [75, 94], in particular, that the same approach should be also applied to the metastable states of He. The additional state with $n_\mathrm{r}=0$ appearing in this case in the total set of states in the subspace of radial functions with a given orbital momentum L has a very low energy and does not virtually affect the Green function and the results of numerical calculations of static susceptibilities. The tensor polarisability and the difference of scalar polarisabilities of the triplet sublevels of He obtained with such model parameters are very sensitive to the quality of the wave functions used and differ from the results of *ab initio* calculations less than by 10 %.

The choice of a closed system of functions of Fues' model potential considerably simplifies and unifies the calculations of the perturbation theory series on the basis of exact analytic expressions for the corresponding characteristics.

5. Analysis of the results of calculation of the second- and fourth-order dynamic susceptibilities

As shown in section 3, the calculations of angular integrals in expressions for matrix elements determining second- and higher-order corrections to the quasi-energy of an atom in the field are performed by standard methods of the quantum theory of the angular momentum of the atom [69] and do not cause any problems (see, for example, [66–68]) and references therein). On the contrary, the calculations of radial matrix elements involve difficulties in the calculation of spectral sums over the complete set of intermediates states including continuum and representing the Green function.

Therefore, a proper choice of the Green function representation that would provide the representation of a final result in the form most convenient for further applications is very important for practical calculations of the polarisability of atomic levels. We calculated radial matrix elements by deriving the Green function for a model potential similarly to the Green function for the Coulomb field (see section 4); for the radial part $g_L^E(r,r')$ appearing in combinations of matrix elements (22), we used the expansion in the Sturm functions (60), which includes only a discrete spectrum. In this case, the expression for individual terms in sums (22)

$$\rho_{L_1}(\pm\omega)=\langle nLSJ|rg_{L_1}^{E_{nLSJ}^{(0)}\pm\omega}(r,r')r'|nLSJ\rangle \quad (63)$$

can be written in the closed analytic form [71]

$$\rho_{L_1}(\pm\omega)=\frac{\nu^3}{16Z^4}\left(\frac{2\nu}{\nu+\nu_n}\right)^{2\lambda_n+4}\left(\frac{2\nu_n}{\nu+\nu_n}\right)^{2\lambda_{L_1}+4}$$

$$\times\frac{\Gamma(1+\nu_n+\lambda_n)}{n_r!\Gamma(2\lambda_{L_1}+2)}\frac{[\Gamma(4+\lambda_n+\lambda_{L_1})]^2}{[\Gamma(2\lambda_n+2)]^2}\times$$

$$\times \sum_{m=0}^{\infty} \frac{(2\lambda_{L_1}+2)_m}{m!(1+m+\lambda_{L_1}-v)} \left[F_2(\lambda_n+\lambda_{L_1}+4; -n_r, -m; 2\lambda_n+2, 2\lambda_{L_1}+2; \frac{2v}{v+v_n}, \frac{2v_n}{v+v_n}) \right]^2. \quad (64)$$

Here, $v = Z/[-2(E^{(0)}_{nLSJ} \pm \omega + \mathrm{i}0)]^{1/2}$; $v_n = Z/(-2E^{(0)}_{nLSJ})^{1/2}$; $\lambda_n = v_n - n_r - 1$ is the orbital parameter [60, 66, 90] of the $|nLSJ\rangle$ state; and F_2 is the Appel function [73]. Compared to the spectral expansion of $\rho_{L_1}(\pm\omega)$ in the eigenfunctions of intermediate states (62), series (64) has a faster convergence, which is explained by the discreteness and equidistance of the eigenvalue spectrum in the generalised Sturm – Liouville problem [97].

The convergence rate of spectral series in the calculation of polarisabilities of alkaline-earth atoms is illustrated in Table 4 by the partial contributions of the spectrum of the intermediate $3snp\,^1P_1$ levels as functions of the principal quantum number obtained by calculating the ground-state polarisability of the Mg atom. The dynamic polarisability was calculated at the 'magic' wavelength $\lambda = 467$ nm. The contributions of the intermediate states with $n = 3 - 10$ were calculated by using the exact oscillator strengths obtained by the multiconfiguration Hartree – Fock method [98, 99]. The levels with $n = 11, ..., \infty$ and the contribution of the continuous spectrum were calculated by the Fues model potential method. Table 4 shows that the consideration of only the first excited states of the intermediate spectrum provides the accuracy of polarisability calculation of the order of a few percent, whereas the contribution of the continuous-spectrum states does not exceed 1 %. However, in some cases the contribution of the continuous spectrum to the polarisability of atomic levels can be quite large (depending on ω and the structure of the ground and excited states of the atom), achieving several tens of percent [100].

Therefore, an important advantage of the Green function method is the possibility to take into account simultaneously contributions from discrete states and continuous-spectrum states in calculations of the atomic polarisability, whereas a direct summation methods involve considerable problems in the estimates of contribution from a continuous spectrum.

As mentioned in Introduction, to realise the light-shift-cancellation regime in optical frequency standards on cold atoms, the polarisation and dispersion properties of the dynamic polarisabilities of levels should be accurately calculated as functions of the power of a laser field forming an optical lattice [24, 25, 29 – 30]. According to expression (50), when the frequency ω is scanned in the vicinity of the intersection point $\omega = \omega_0$ of dynamic polarisabilities corresponding to the 'magic' wavelength λ_0, the second-order dynamic Stark effect is completely mutually compensated, and therefore the perturbation of the $^1S_0 - {}^3P_J$ ($J = 0, 1, 2$) clock transition by the laser field of the optical lattice is caused only by the higher-order terms [fourth-order dynamic susceptibilities (hyperpolarisabilities) and relativistic corrections to the operator of electric dipole interaction with the laser radiation field].

It is well known from the literature [101, 102] that the dispersion properties of the dynamic polarisability in the region between resonances depend not only on the frequency and polarisation of the laser field but also on the structure of the atomic levels under study. Thus, in the case of a linearly polarised field, the dynamic polarisability of the ground state of atoms has a single node in each region between resonances.

The behaviour of polarisabilities of excited atoms can drastically change; in particular, the polarisability may either have no nodes or may have two nodes in each region between resonances (changing its sign across each resonance). These dispersion properties are explained by the possibility of resonances of the levels under study both with high-lying and low-lying atomic levels. The behaviour of polarisabilities of high excited Rydberg atomic levels in a monochromatic field is described in [72, 92, 101].

On the other hand, the laser radiation frequency ω_0 at which the light shift is mutually compensated should satisfy the two basic conditions [25, 31]:

(i) the intersection point of dynamic polarisabilities should be located as far as possible from the resonance to minimise the resonance absorption and scattering of laser radiation forming an optical lattice;

(ii) the decay probability of the excited ^3P_J level ($J = 0$, 1, 2) due to two-photon ionisation at the frequency ω_0 should be negligible compared to the probability of one-photon decay to the ground state.

Table 4. Contributions of the intermediate $3snp\,^1P_1$ levels to the dipole static and dynamic polarisabilities of the Mg atom in the ground state.

n	Energy difference in the absence of the field ΔE ($3s^2\,^1S_0 - 3snp\,^1P_1$)/cm^{-1}	Static polarisability/au		Dynamic polarisability/au	
		$3snp\,^1P_1$ level	Spectral sum	$3snp\,^1P_1$ level	Spectral sum
3	35051	67.801	67.80	108.17	108.1
4	49346	2.412	70.21	2.97	111.1
5	54706	0.455	70.66	0.53	111.6
6	57214	0.150	70.81	0.17	111.8
7	58580	0.068	70.88	0.07	111.9
8	59403	0.036	70.92	0.04	111.9
9	59936	0.022	70.94	0.02	112.0
10	60302	0.014	70.96	0.01	112.0
$11, ..., \infty$		0.020	70.98	0.02	112.1
Continuous spectrum		0.41	71.39	0.4	112.4

By using theoretical expressions from previous sections and taking into account the above-mentioned conditions, we calculated the dynamic polarisabilities of the $^1S_0$ ground and the $^3P_0$ excited levels for the fermion isotope of the Sr atom in the vicinity of the 'magic' wavelength $\lambda_0 \approx 800$ nm (Fig. 3). The laser radiation field was assumed linearly polarised and its intensity was set equal to 10 kW cm^{-2}. The dynamic polarisabilities were calculated by two independent methods: the use of the Sturm-series expansion for the Green function in the Fues model potential and by the direct summation method taking into account the discrete-spectrum levels with $n \leqslant 10$. In the latter case, we used the exact matrix elements of the dipole moment calculated by the multiconfiguration Hartree–Fock method [25, 103]. These calculations showed that the compared values coincided within 2 %–3 %, thus confirming the reliability of calculations. We have shown [25] that hyperfine structure effects and the dependence of the light shift on the laser-field polarisation are insignificant due to the zero electronic momenta of the ground and excited states and do not affect the value of λ_0 in the calculations of dynamic polarisabilities of the Sr atom. The contribution of the continuous-spectrum states is also small and does not exceed 1 %. However, the value of $\lambda_0 = 813 \pm 2$ nm measured in [31] exceeds somewhat the above estimates. The reason for the discrepancy between the experimental data and theoretical calculations obtained by independent methods is not clear and is being discussed at present.

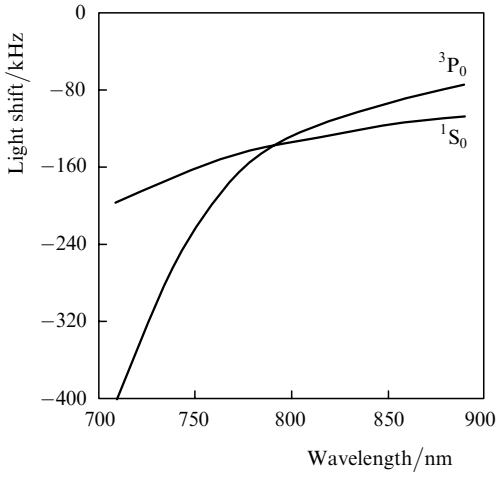

Figure 3. Light shift for the $^1S_0$ and $^3P_0$ levels in the Sr atom in the vicinity of the 'magic' wavelength λ_0 of a linearly polarised field.

Because no experimental data on the high-order shifts of atomic levels in a light field are available in the literature, we performed theoretical estimates of these shifts for the forbidden $^3P_0 - {}^1S_0$ transition in the Sr atom. Despite a comparatively low power of lasers used in experiments (of the order of a few tens of kilowatts per square centimetre), these estimates are principally important because after the mutual compensation of the second-order field corrections, the fourth-order light shift described by the dynamic hyperpolarisabilities of levels is one of the main sources of systematic uncertainties in measurements of the clock transition frequency in the optical frequency standards of this type. Therefore, interest in the correction term $-(E_0^4/64)\Delta\gamma(\boldsymbol{e},\omega)$ in expression (50), determining the deviation of the dependence of the light frequency shift from quadratic, is caused by the requirement to analyse the metrological characteristics of optical frequency standards with the relative error $10^{-16} - 10^{-18}$.

Unlike a static field, for the laser-wave field it is rather difficult to formulate the unified criteria for estimating the contribution of the high orders of the perturbation theory because the calculated dynamic hyperpolarisabilities more strongly depend on the filed frequency than the second-order light shifts. Moreover, along with one-photon resonances discussed above, two-photon resonances of $\Delta\gamma(\boldsymbol{e},\omega)$ also appear on the intermediate levels of the same parity as the parity of the level under study. In the general case, the number of different resonances and their dispersion properties substantially depend on the type of laser-field polarisation [67].

Although the general expressions for dynamic hyperpolarisabilities are rather cumbersome [67, 68, 75], nevertheless they can be written for specific states as a combination of the irreducible components of the fourth-rank tensor. In particular, for a linearly polarised field, the dynamic hyperpolarisability is determined by three invariant parameters, and for a circularly polarised field – by five parameters, all of them being represented by the fourth- and second-order reduced matrix elements of the dipole moment operator [67]:

$$R_{J_1J_2J_3}(\omega_1,\omega_2,\omega_3)$$

$$= \langle \beta J \| \boldsymbol{D} G_{J_1}^{E_{\beta J}+\omega_1} \boldsymbol{D} G_{J_2}^{E_{\beta J}+\omega_2} \boldsymbol{D} G_{J_3}^{E_{\beta J}+\omega_3} \boldsymbol{D} \| \beta J \rangle, \qquad (65)$$

$$R_{J_1J_2}(\omega) = \langle \beta J \| \boldsymbol{D} G_{J_1}^{E_{\beta J}+\omega} G_{J_1}^{E_{\beta J}+\omega} \boldsymbol{D} \| \beta J \rangle, \qquad (66)$$

$$R_{J_1}(\omega) = \langle \beta J \| \boldsymbol{D} G_{J_1}^{E_{\beta J}+\omega} \boldsymbol{D} \| \beta J \rangle. \qquad (67)$$

The frequencies ω_{1-3} in (65) satisfy the conditions

$$\omega_1, \omega_3 = \pm\omega, \quad \omega_2 = 0, \pm 2\omega. \qquad (68)$$

Integration over radial variables in (65)–(67) by using the Sturm expansion for the Green function is also performed by analytic methods, and the final result is written as a combination of rapidly converging series containing the hypergeometric Gaussian functions ${}_2F_1$ [73]. Our calculations of the hyperpolarisabilities for a linearly polarised field at the 'magic' laser wavelength $\lambda_0 \approx 800$ nm gave the values [25]

$$\gamma(^1S_0) = 6.3 \times 10^6 \text{ au}, \qquad (69)$$

$$\gamma(^3P_0) = 2.7 \times 10^8 \text{ au} \qquad (70)$$

The fourth-order corrections to the light shift of levels in the frequency units for the field intensity 10 kW cm^{-2} are [25]

$$\Delta E^{(4)}(^1S_0) \approx -5.3 \times 10^{-5} \text{ Hz}, \qquad (71)$$

$$\Delta E^{(4)}(^3P_0) \approx -2.3 \times 10^{-3}\text{Hz}. \quad (72)$$

Therefore, after the mutual compensation of the second-order field corrections, the relative contribution of the dynamic Stark effect to the frequency of the $^1S_0 - {}^3P_0$ clock transition does not exceed 10^{-17}.

We also estimated the effects of magnetic dipole (V_μ) and electric quadrupole (V_Q) interactions of the Sr atom with an external monochromatic field. These estimates showed that the relation between the magnetic dipole, electric quadrupole, and electric dipole polarisabilities can be represented in the form [25]

$$\alpha_{M1}(\omega_0) \approx \alpha_{E2}(\omega_0) \approx 10^{-7}\alpha_{E1}(\omega_0) \quad (73)$$

and, hence, the relative contribution of high-multipolarity corrections to the $^3P_0 - {}^1S_0$ transition frequency also does not exceed 10^{-17}.

By using the method discussed in sections 3 and 4, we performed systematic calculations of the dynamic polarisabilities of some other systems of interest for modern frequency standards on cold atoms. The Stark shift of the clock levels was estimated assuming in all cases (except the Mg atom) that the laser field intensity was 10 kW cm^{-2}.

As pointed out above (Tables 2 and 3), the Yb atom has two stable odd isotopes, ^{171}Yb and ^{173}Yb for which the probability of the $^1S_0 - {}^3P_0$ transition induced by the hyperfine structure effect and singlet–triplet mixing of the $^3P_1$ and $^1P_1$ levels is nonzero (Table 3). The lifetime of these atoms is tens of seconds, which makes them promising working media for optical frequency standards at 578 nm [104]. Table 5 presents the dynamic polarisabilities calculated for the $^1S_0$ and $^3P_0$ levels of the Yb atom as functions of the wavelength of a linearly polarised laser field. The calculations by the Fues model potential method were performed in two ways: by using the Green function formalism for intermediate states (α^G) and by the method of direct summation (α^{ds}) over the spectrum of intermediate states within the specified accuracy of the theoretical calculation $\sim 10^{-4}$. The data presented in Table 5 show that the results obtained by these methods are in good agreement (within a few percent) over the entire wavelength range considered, and the 'magic' wavelength λ_0 at the $^1S_0 - {}^3P_0$ transition is ~ 724 nm.

The static polarisabilities of the Yb atom in the ground state $\alpha^G(^1S_0) = 121.2$ au and $\alpha^{ds}(^1S_0) = 120.6$ au do not differ from the calculated precision Hartree–Fock value $\alpha^{HF}(^1S_0) = 118 \pm 45$ au within the accepted accuracy [105]. However, for the excited $^3P_0$ level, the difference amounts to 40 %: $\alpha^G(^3P_0) = 351.5$ au, $\alpha^{ds}(^3P_0) = 350.5$ au, and $\alpha^{HF}(^3P_0) = 252 \pm 25$ au [105].

We also estimated the contribution of electrons of the atomic core to the dynamic Stark effect in the Yb atom [85, 86]. Within the framework of the Fues model potential in the multichannel approximation (which is in fact the multichannel analogue of the quantum defect method in complex atoms [106]), we calculated the light shift of the $(4f^{14})6s6p(^3P_0)$ level of Yb at $\lambda = 532$ nm. The calculated shift $\Delta E^{(2)}(^3P_0) \approx -125$ kHz is of interest in itself for experimental studies performed at the University of Kyoto, Japan [107]. The use of the model potential method in the multichannel approach for estimating the 'magic' wavelength at the $^1S_0 - {}^3P_0$ transition gives $\lambda_0 \approx 750$ nm, which virtually coincides with the value $\lambda_0 \approx 752$ nm calculated in [57]. Note that, along with a small change in the 'magic' wavelength (750 nm instead of 724 nm), the consideration of the contribution of the electrons of the $4f^{14}$ shell leads to an increase in the polarisability and, hence, the depth of the Stark potential of the optical lattice by more than twice (−200 kHz instead of −80 kHz) [56, 85, 86].

Table 5. Dynamic polarisabilities for the ground $[(4f^{14})6s^2\,{}^1S_0]$ and excited $[(4f^{14})6s6p\,{}^3P_0]$ levels of the Yb atom calculated by the model potential Green function method (α^G) and the method of direct summation (α^{ds}) over the intermediate states of the discrete spectrum [the first term in the right-hand side in (62)].

Wavelength/nm	$\alpha^G(^1S_0)$/au	$\alpha^{ds}(^1S)$/au	$\alpha^G(^3P_0)$/au	$\alpha^{ds}(^3P_0)$/au
650	192.5	191.9	22683.1	22682.3
660	189.2	188.5	1829.2	1828.1
670	186.1	185.4	914.6	913.6
680	183.2	182.5	588.7	587.6
690	180.5	179.9	419.7	418.6
700	178.0	177.4	315.0	314.0
710	175.7	175.1	242.9	241.8
720	173.5	172.9	189.5	188.5
721	173.3	172.7	184.9	183.8
722	173.1	172.5	180.4	179.3
723	172.9	172.3	176.0	174.9
724*	172.7	172.1	171.7	170.6
725	172.5	171.9	167.5	166.5
726	172.3	171.7	163.4	162.4
727	172.1	171.5	159.3	158.3
728	171.9	171.3	155.4	154.4
729	171.7	171.1	151.6	150.6
730	171.5	170.9	147.8	146.8
740	169.6	169.0	113.9	112.9
750	167.8	167.2	85.4	84.3
760	166.1	165.5	60.7	59.7
770	164.5	163.9	38.9	37.9
780	163.0	162.4	19.3	18.3
790	161.6	161.0	1.3	0.3
800	160.3	159.7	−15.4	−16.4

*Note: 'magic' wavelength at the $^1S_0 - {}^3P_0$ transition in the Yb atom.

Figure 4 presents the dispersion and polarisation dependences of the light frequency shift for forbidden optical transitions in the Mg atom. Unlike the previous calculations, the laser field intensity was assumed equal to 3.5 MW cm^{-2}, in accordance with the requirements of experiments being performed and planned at the Technical University of Hanover, Germany [26].

Figure 4a shows the light shift for the $^1S_0 - {}^3P_0$ transition in the wavelength range from 350 to 700 nm. As follows from section 3, the contributions of the ^3S term of the intermediate spectrum to the scalar and tensor components of the dynamic polarisability of the $^3P_1$ ($M = 0$) level are mutually compensated and the resonance features of the light shift are determined by the contribution of the ^3D levels of the intermediate spectrum. The intersection point of dynamic polarisabilities is located between two ^3D resonances, and the corresponding 'magic' wavelength at this transition is $\lambda_0 \approx 312$ nm (Fig. 4b). For the $^1S_0 - {}^3P_1$ transition with $M \neq 0$, on the contrary, the situation is

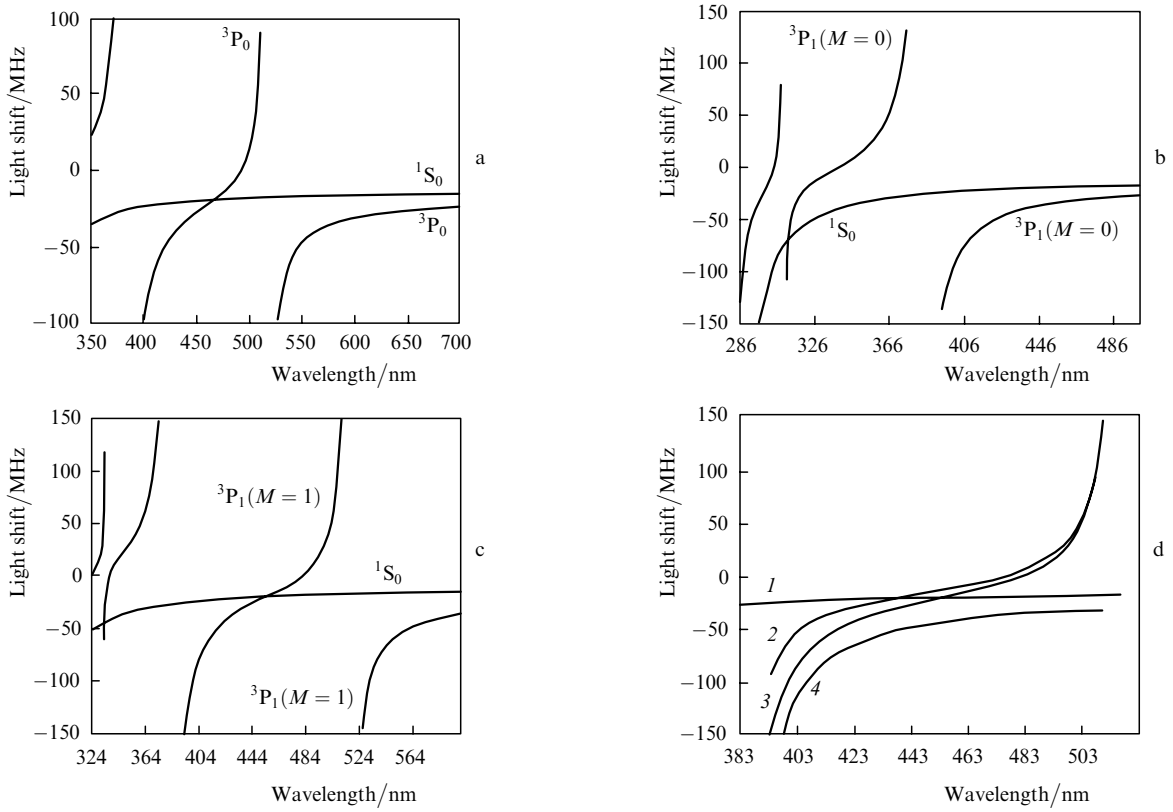

Figure 4. Dynamic Stark effect for the $^1S_0$ and $^3P_0$ (a), $^1S_0$ and $^3P_1(M=0)$ (b) and $^1S_0$ and $^3P_1(M=1)$ (c) levels in the Mg atom for a linearly polarised field and also the polarisation and dispersion dependences of the dynamic polarisabilities of the $^1S_0$ and $^3P_1(M=1)$ levels in the wavelength range between the 517.2-nm ^3S resonance and 383.3-nm ^3D resonance for the ground state (*1*) and the $^3P_1(M=1)$ level for linear (*2*), right-hand (*3*), and left-hand (*4*) circular polarisations (d).

substantially different, and the intersection point of dynamic polarisabilities is located in the region between resonances formed by the ^3S and ^3D terms of the spectrum of intermediate states (Fig. 4c). Figure 4d shows the dispersion dependences for the $^3P_1$ ($M=1$) level of the Mg atom for the linear, right- and left-hand circular polarisations of the laser field. By using expression (40), we can easily show that the dynamic polarisability calculated for the $^3P_1$ ($M=-1$) level is completely identical to the polarisability of the $^3P_1$ ($M=1$) level calculated for the case of right-hand circular polarisation (Fig. 4d). The analysis of polarisation dependences of the dynamic polarisability (Fig. 4d) shows that the laser-field polarisation noticeably affects both the dispersion properties of the light shifts of atomic levels and the position of their intersection points.

We also calculated the light shifts for He, Be, Ca, and Hg atoms. The results of these calculations are presented in Figs 5–8.

6. Conclusions

This study was initiated by the problems of the development of highly stable optical frequency standards of a new generation based on the intercombination and hyperfine-interaction-induced clock $^1S_0 - {}^3P_J$ ($J=0,1$) transitions in cold alkaline-earth atoms. For optical standards of this type, the 'light-shift-cancellation' regime (first proposed and realised at the University of Tokyo, Japan) was studied theoretically for the Sr atom [24, 25, 29–31]. In this regime, the quadratic Stark shifts of the ground and excited levels

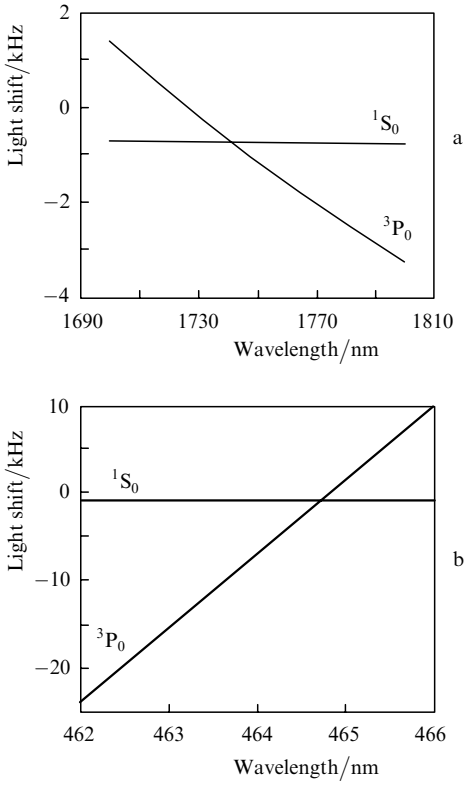

Figure 5. Light shifts for the $^1S_0$ and $^3P_0$ levels in the He atom in the vicinity of the 'magic' wavelengths $\lambda_0 = 1739$ (a) and 465 nm (b).

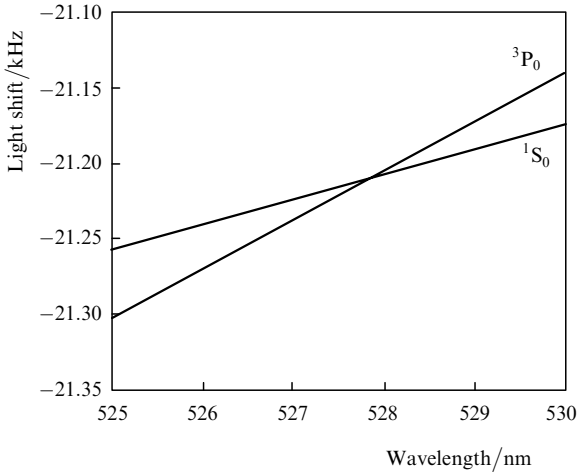

Figure 6. Light shifts for the $^1S_0$ and $^3P_0$ levels in the Be atom.

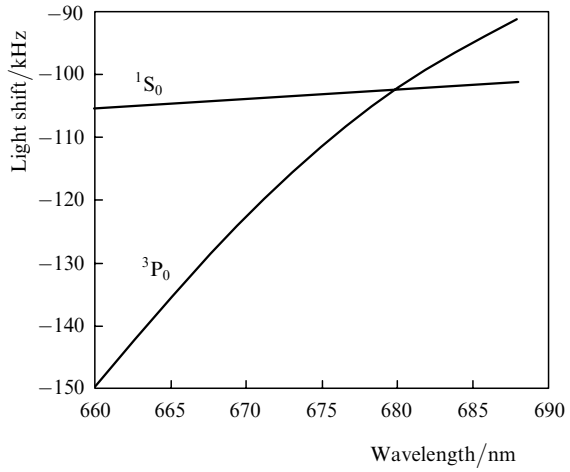

Figure 7. Light shifts for the $^1S_0$ and $^3P_0$ levels in the Ca atom.

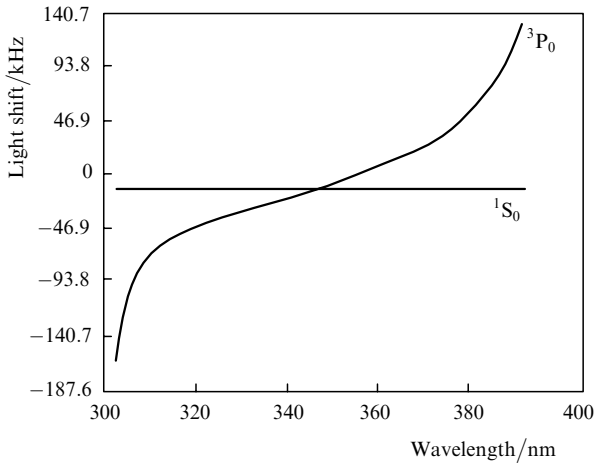

Figure 8. Light shifts for the $^1S_0$ and $^3P_0$ levels in the Hg atom in the vicinity of the 'magic' wavelength $\lambda_0 = 342$ nm.

trapped in the optical lattice are completely mutually compensated.

We have calculated in detail the light frequency shifts in He, Be, Mg, Ca, Sr, Yb, and Hg atoms as functions of the frequency, intensity, and polarisation of the laser field producing the optical lattice. Calculations were performed by using the perturbation theory for the quasi-energy levels of atoms in an external monochromatic field taking into account the terms of the second and fourth orders in the laser radiation amplitude. The main characteristics determining variations of the atomic spectrum in the laser field are the dynamic polarisabilities and hyperpolarisabilities of levels represented as a sum of irreducible tensor components of these quantities.

By analysing the dispersion and polarisation properties of dynamic polarisabilities of atoms, we determined the 'magic' laser wavelengths at which the quadratic Stark shifts in the initial and final states are mutually compensated. We also have demonstrated the efficiency of the Green function method for Fues' model potential for calculating dynamic polarisabilities and accurate estimates of the high-order effects (dynamic hyperpolarisabilities, magnetic dipole, and electric quadrupole corrections to the dipole polarisability), which are one of the main sources of systematic errors in optical frequency standards of this type.

The calculations performed for the fermion isotope of Sr have shown that the relative contribution of high-order effects at the $5s^2\,{}^1S_0\,(F = 9/2) - 5s5p\,{}^3P_0\,(F = 9/2)$ transition does not exceed $\sim 10^{-17}$ for a linearly polarised laser field of intensity 10 kW cm^{-2} ($\lambda_0 \approx 800$ nm). This circumstance makes it possible in principle to obtain the unique metrological characteristics of optical frequency standards on cold neutral atoms (the line Q factor as high as 10^{12}–10^{14}, and the accuracy and stability amounting to $10^{-16} - 10^{-18}$).

References

1. Jefferts S.R., Meekhof D.M., Heavner T.P., Parker T.E. *Metrologia*, **39**, 321 (2002).
2. Weyers S., Hübner U., Schröder R., Tamm Chr., Bauch A. *Metrologia*, **38**, 343 (2001).
3. Pereira Dos Santos F., Marion H., Abgrall M., Zhang S., Sortais Y., Bize S., Maksimovic I., Calonico D., Grunert J., Mandache C., Vian C., Rosenbuch P., Lemonde P., Santarelli G., Clairon A. *Proc. 2003 IEEE Int. Frequency Control Symp. and PDA Exhibition jointly with the 17th Europ. Frequency and Time Forum* (Tampa, USA, 2003) pp 55–67.
4. Marion H., Pereira Dos Santos F., Abgrall M., Zhang S., Sortais Y., Bize S., Maksimovic I., Calonico D., Grunert J., Mandache C., Lemonde P., Santarelli G., Laurent P., Clairon A., Salomon C. *Phys. Rev. Lett.*, **90**, 150801 (2003).
5. Levi F., Lorini L., Calonico D., Godone A. *IEEE Trans. Ultrason Ferroelectrics Frequency Control*, **51**, 1216 (2004).
6. Szymaniec K., Chalupczak W., Whilberley P.B., Lea S.N., Henderson D. *Metrologia*, **42**, 49 (2005).
7. Vanier J., Audoin C. *Metrologia*, **42**, S31 (2005).
8. Bauch A. *Metrologia*, **42**, S43 (2005).
9. Domnin Yu., Gaigerov B., Kochelyaevsky N., Poushkin S., Rusin F., Tatarenkov V., Yolkin G. *Metrologia*, **42**, S55 (2005).
10. Wynands R., Weyers S. *Metrologia*, **42**, S64 (2005).
11. Bagayev S.N., Zakhar'yash V.F., Klement'ev V.M., Kolker D.B., Kuznetsov S.A., Matyugin E.A., Pivtsov V.S., Skvortsov M.N., Chepurov S.V. *Kvantovaya Elektron.*, **31**, 383 (2001) [*Quantum Electron.*, **31**, 383 (2001)].
12. Stenger J., Schnatz H., Tamm C., Telle H.R. *Phys. Rev. Lett.*, **88**, 073601 (2002).
13. Baklanov E.V., Pokasov P.V. *Kvantovaya Elektron.*, **33**, 383 (2003) [*Quantum Electron.*, **33**, 383 (2003)].
14. Jones R.J., Diels J.C. *Phys. Rev. Lett.*, **86**, 3288 (2001).
15. Diddams S.A., Jones R.J., Ye J., Cundiff S.T., Hall J.L., Ranka J.K., Windeler R.S., Holzwarth R., Udem T., Hansch T.W. *Phys. Rev. Lett.*, **84**, 5102 (2000).

16. Bagayev S.N., Denisov V.I., Zakhar'yash V.F., Kashirskii A.V., Klement'ev V.M., Kuznetsov S.A., Korol' I.I., Pivtsov V.S. *Kvantovaya Elektron.*, **34**, 1096 (2004) [*Quantum Electron.*, **34**, 1096 (2004)].
17. Hollberg L., Diddams S., Bartels A., Fortier T., Kim K. *Metrologia*, **42**, S105 (2005).
18. Reichert J., Niering M., Holzwarth R., Weitz M., Udem Th., Hänsch T.W. *Phys. Rev. Lett.*, **84**, 3232 (2000).
19. Wilpers G., Binnewies T., Dagenhardt C., Helmcke J., Riehle F. *Phys. Rev. Lett.*, **89**, 230801 (2002).
20. Gill P., Barwood G.P., Huang G., Klein H.A., Blythe P.J., Hosaka K., Thompson R.C., Webster S.A., Lea S.N., Margolis H.S. *Physica Scripta T*, **112**, 63 (2004).
21. Yoon T.H., Ye J., Hall J.L., Chartier J.M. *Appl. Phys. B*, **72**, 221 (2001).
22. Gill P. *Metrologia*, **42**, S125 (2005).
23. Tamm Chr., Schneider T., Peik E., in *Laser Spectroscopy* (Singapore: World Scientific, 2004) Vol. XVI, pp 57–61.
24. Katori H., Ido T., Kuwata-Gonokami M. *J. Phys. Soc. Jpn.*, **68**, 2479 (1999).
25. Katori H., Takamoto M., Pal'chukov V.G., Ovsiannikov V.D. *Phys. Rev. Lett.*, **91**, 173005 (2003).
26. Binnewies T., Wilpers G., Sterr U., Riehle F., Helmcke J., Mehlstäubler T.E., Rasel E.M., Ertmer W. *Phys. Rev. Lett.*, **87**, 123002 (2001).
27. Poli N., Drullinger R.E., Ferrari G., Leonard J., Sorrentino F., Tino G.M. *Phys. Rev. A*, **71**, 061403(R) (2005).
28. Rafac R.J., Young B.C., Beall J.A., Itano W.M., Wineland D.J., Bergquist J.C. *Phys. Rev. Lett.*, **85**, 2462 (2000).
29. Katori H. *Proc. 6th Symp. on Frequency Standards and Metrology* (Singapore: World Scientific, 2002) pp 323–330.
30. Katori H., Ido T., Isoya Y., Kuwata-Gonokami M. *Phys. Rev. Lett.*, **82**, 1116 (1999).
31. Takamoto M., Katori H. *Phys. Rev. Lett.*, **91**, 223001 (2003).
32. Letokhov V.S. *Pis'ma Zh. Eksp. Teor. Fiz.*, **7**, 348 (1968).
33. Dicke R.M. *Phys. Rev.*, **89**, 472 (1953).
34. Mukaiyama T., Katori H., Ido T., Li Y., Kuwata-Gonokami M. *Phys. Rev. Lett.*, **90**, 113002 (2003).
35. Sobel'man I.I. *Vvedenie v teoriyu atomnykh spektrov* (Introduction to the Theory of Atomic Spectra) (Moscow: Nauka, 1977).
36. Johnson W.R., Plante D.R., Sapirstein J. *Adv. At. Mol. Phys.*, **35**, 255 (1995).
37. Savukov I.M., Johnson W.R. *Phys. Rev. A*, **65**, 042503 (2002).
38. Derevianko A. *Phys. Rev. Lett.*, **87**, 023002 (2001).
39. Santra R., Christ K.V., Greene C.H. *Phys. Rev. A*, **69**, 042510 (2004).
40. Porsev S.G., Kozlov M.G., Rakhlina Y.G., Derevianko A. *Phys. Rev. A*, **64**, 012508 (2001).
41. Godone A., Novero C. *Phys. Rev. A*, **65**, 1717 (1992).
42. Kwong H.S., Smith P.L., Parkinson W.H. *Phys. Rev. A*, **25**, 2629 (1982).
43. Mitchel C.J. *J. Phys. B*, **8**, 25 (1975).
44. Husain D., Roberts G.J. *J. Chem. Soc. Faraday Trans. 2*, **82**, 1921 (1986).
45. Drozdowski R., Ignasiuk M., Kwela J., Heldt J. *Z. Phys. D: At. Mol. Clusters*, **41**, 125 (1997).
46. Whitkop P.G., Wiesenfeld J.R. *Chem. Phys. Lett.*, **80**, 321 (1984).
47. Husain D., Schifino J. *J. Chem. Soc. Faraday Trans. 2*, **80**, 321 (1984).
48. Kelly J.F., Harris M., Gallagher A. *Phys. Rev. A*, **37**, 2354 (1988).
49. Jönsson P., Fiescher C.F. *J. Phys. B*, **30**, 5861 (1997).
50. Garstang R.G. *Astrophys. J.*, **148**, 579 (1967).
51. Mizushima M. *Phys. Rev. A*, **134**, 883 (1964).
52. Porsev S.G., Derevianko A. *Phys. Rev. A*, **69**, 042506 (2004).
53. Bergström H., Levinson C., Lundberg H., Svanberg S., Wahlström C.G., Zhao You Yuan. *Phys. Rev. A*, **33**, 2387 (1986).
54. Brage T., Judge P.G., Aboussaid A., Godefroid M.R., Jonsson P., Ynnerman A., Fiescher C.F., Leckrone D.S. *Astrophys. J.*, **500**, 507 (1998).
55. Garstang R.G. *J. Opt. Soc. Am.*, **37**, 845 (1962).
56. Pal'chikov V.G. *Proc. 15th Europ. Frequency and Time Forum (EFTF-2002)* (St.Petersburg, Russia, 2002) pp 132–136.
57. Porsev S.G., Derevianko A., Fortson E.N. *Phys. Rev. A*, **69**, 021403 (2004).
58. Zel'dovich Ya.B. *Usp Fiz. Nauk*, **110**, 139 (1973).
59. Zel'dovich Ya.B., Manakov N.L., Rapoport L.P. *Usp Fiz. Nauk*, **117**, 563 (1975).
60. Rapoport L.P., Zon B.A., Manakov N.L. *Teoriya mnogofotonnykh protsessov v atomakh* (Theory of Multiphoton Processes in Atoms) (Moscow: Atomizdat, 1978).
61. Manakov N.L., Fainshtein A.G. *Dokl. Akad. Nauk SSSR*, **244**, 567 (1979).
62. Manakov N.L., Fainshtein A.G. *Zh. Eksp. Teor. Fiz.*, **79**, 751 (1980).
63. Manakov N.L., Preobrazhenskii M.A., Rapoport L.P., Fainshtein A.G. *Zh. Eksp. Teor. Fiz.*, **75**, 1243 (1978).
64. Manakov N.L., Fainshtein A.G. *Teor. Mat. Fiz.*, **78**, 385 (1981).
65. Manakov N.L, Marmo S.I., Pronin E.A. *Zh. Eksp. Teor. Fiz.*, **125**, 288 (2004).
66. Manakov N.L., Ovsiannikov V.D., Rapoport L.P. *Phys. Rep.*, **141**, 319 (1986).
67. Davydkin V.A., Ovsiannikov V.D. *J. Phys. B*, **19**, 2071 (1986).
68. Bolgova I.L., Ovsiannikov V.D., Pal'chikov V.G., Magunov A.I., von Oppen G. *Zh. Eksp. Teor. Fiz.*, **123**, 1145 (2003).
69. Varshalovich D.A., Moskalev A.N., Khersonskii V.K. *Kvantovaya teoriya uglovogo momenta* (Quantum Theory of Angular Momentum) (Leningrad: Nauka, 1975).
70. Angel J.R.P., Sandars P.G.H. *Proc. Roy. Soc. A*, **305**, 125 (1968).
71. Manakov N.L., Ovsiannikov V.D. *J. Phys. B*, **10**, 569 (1977).
72. Davydkin V.A., Ovsiannikov V.D., Zon B.A. *Laser Phys.*, **3**, 449 (1993).
73. Erdelyi A. (Ed.) *Higher Transcendental Functions (Bateman Manuscript Project)* (New York: McGraw-Hill, 1953; Moscow: Nauka, 1965) Vol. 1.
74. Davydkin V.A., Ovsiannikov V.D. *J. Phys. B*, **17**, L207 (1984).
75. Derevianko A., Johnson W.R., Ovsiannikov V.D., Pal'chikov V.G., Plante D.R., von Oppen G. *Phys. Rev. A*, **60**, 986 (1999).
76. Itano W.M., Lewis L.L., Wineland D.J. *Phys. Rev. A*, **35**, 1233 (1982).
77. Manakov N.L., Rapoport L.P., Zapryagaev S.A. *Phys. Lett. A*, **48**, 145 (1974).
78. Micalizio S., Godone A., Colonico D., Levi F., Lorini L. *Phys. Rev. A*, **69**, 053401 (2004).
79. Pal'chikov V.G. *Hyperfine Interaction*, **127**, 287 (2000).
80. Johnson W.R., Cheng R.T. *Phys. Rev. A*, **53**, 1375 (1996).
81. Cheng R.T., Chen M.H., Johnson W.R., Sapirstein J. *Phys. Rev. A*, **50**, 247 (1994).
82. Abarenkov I.V., Heine I. *Philos. Mag.*, **12**, 529 (1965).
83. Laughlin C., Victor G.A. *Adv. Atomic Molecular Phys.*, **25**, 163 (1988).
84. Patil S.H. *Europhys. J. B*, **10**, 341 (2000).
85. Pal'chikov V.G., Ovsiannikov V.D. *Kvantovaya Elektron.*, **34**, 412 (2004) [*Quantum Electron.*, **34**, 412 (2004)].
86. Pal'chikov V.G., Ovsiannikov V.D. *Proc. SPIE Int. Soc. Opt. Eng.*, **5478**, 219 (2004).
87. Simons G. *J. Chem. Phys.*, **55**, 756 (1971).
88. Simons G. *J. Chem. Phys.*, **60**, 645 (1974).
89. Simons G., Martin J. *J. Chem. Phys.*, **62**, 4799 (1975).
90. Manakov N.L., Ovsiannikov V.D., Rapoport L.P. *Opt. Spektr.*, **38**, 206 (1975).
91. Manakov N.L., Marmo S.I., Fainshtein A.G. *Teor. Mat. Fiz.*, **79**, 44 (1984); *Zh. Eksp. Teor. Fiz.*, **91**, 51 (1986).
92. Krylovetskii A.A., Manakov N.L., Marmo S.I. *Zh. Eksp. Teor. Fiz.*, **119**, 45 (2001).
93. Manakov N.L., Maquet A., Marmo S.I., Szymanowski C. *Phys. Lett. A*, **237**, 234 (1998).
94. Derevianko A., Johnson W.R., Ovsiannikov V.D., Pal'chikov V.G., Plante D.R., von Oppen G. *Zh. Eksp. Teor. Fiz.*, **115**, 494 (1999).

95. Derevianko A., Johnson W.R., Ovsiannikov V.D., Pal'chikov V.G., Plante D.R., von Oppen G. *Proc. Int. Conf on Atomic Phys. (ICAP-98)* (Winsor, Canada, 1999) p. 215.
96. Seaton M.J. *Rep. Prog. Phys.*, **46**, 167 (1983).
97. Khristenko S.V. *Teor. Mat. Fiz.*, **2**, 31 (1975).
98. Tachiev G., Froese Fischer C. *J. Phys. B*, 32, 586 (1999).
99. Chang T.N. *Phys. Rev. A*, **41**, 4922 (1990).
100. Amus'ya M.Ya., Cherepkov N.A., Shapiro S.G. *Zh. Eksp. Teor. Fiz.*, **63**, 889 (1972).
101. Delone N.B., Krainov V.P., Shepelyanskii D.L. *Usp. Fiz. Nauk*, **140**, 355 (1983).
102. Delone N.B., Krainov V.P. *Atom v sil'nom svetovom pole* (Atom in a Strong Light Field) (Moscow: Energoatomizdat, 1984).
103. Pal'chikov V.G., Domnin Yu.S., Novoselov A.V. *J. Opt. B: Quantum Semiclass.*, **5**, S131 (2003).
104. Park C.Y., Yoon T.H. *Phys. Rev. A*, **68**, 055401 (2003).
105. Porsev S.G., Rakhlina Yu.G., Kozlov M.G. *Phys. Rev. A*, **60**, 2781 (1999).
106. Aymar M., Greene C.H., Lue-Koenig E. *Rev. Mod. Phys*, **68**, 1014 (1996).
107. Takahashi Y., private communication (2005).